Influence of pyrolysis temperature on the characteristics and lead(II) adsorption capacity of phosphorus-engineered poplar sawdust biochar

Yonggang Xu[a], Tianxia Bai[b], Qiao Li[c], Hongtao Yang[d],Yubo Yan[b*], Binoy Sarkar[e*], Su Shiung Lam[f], Nanthi Bolan[g]

[a]*Jiangsu Key Laboratory for Eco-Agricultural Biotechnology around Hongze Lake/ Collaborative Innovation Center of Regional Modern Agriculture & Environmental Protection, Huaiyin Normal University, Huai'an, 223300, China*

[b]*School of Chemistry and Chemical Engineering, Huaiyin Normal University, Huai'an, 223300, China*

[c]*School of Environmental and Biological Engineering, Nanjing University of Science and Technology, Nanjing 210094, China*

[d]*Xi'an Modern Chemistry Research Institute, Xi'an 71065, PR China*

[e]*Lancaster Environment Centre, Lancaster University, Lancaster, LA1 4YQ, United Kingdom*

[f]*Pyrolysis Technology Research Group, Institute of Tropical Aquaculture and Fisheries (AKUATROP) & Institute of Tropical Biodiversity and Sustainable Development (Bio-D Tropika), Universiti Malaysia Terengganu, 21030 Kuala Nerus, Terengganu, Malaysia*

[g]*Faculty of Science, The University of Newcastle, University Drive, Callaghan, NSW 2308, Australia*

***Corresponding author:**

Dr Yubo Yan (yubo.yan@hytc.edu.cn); Dr Binoy Sarkar (b.sarkar@lancaster.ac.uk)

Abstract

Phosphorus (P)-engineered biochars (BCP) were prepared via co-pyrolysis of poplar sawdust and monopotassium phosphate (KH_2PO_4) (10%, w/w) at 300 °C, 500 °C and 700 °C to evaluate their potential lead [Pb(II)] adsorption. Effects of pH, contact time, and initial Pb(II) concentration on the Pb(II) adsorption capacity of the biochars were investigated. The physico-chemical, morphological, porous structure, crystallinity and spectroscopic characteristics of pre- and post-Pb-adsorbed biochars were analyzed to unravel the Pb(II) adsorption mechanism.

Results showed that KH_2PO_4 reacted with biomass carbon to form stable C-P and/or C-O-P groups in BCP, and increased carbon retention and aromaticity of BCP. However, the addition of KH_2PO_4 led to an adverse effect on porous structure, e.g. surface area of biochars produced at 300 °C, 500 °C and 700 °C were decreased by 41.53%, 80.32%, and 59.74%, respectively. Adsorption experiments displayed that BCP produced at 300 °C exhibited the highest Pb(II) adsorption capacity (q_{max}=154.7 mg g^{-1}), which was almost 6 times higher than the pristine biochar (q_{max}= 24.3 mg g^{-1}). Potassium polymetaphosphate [$(KPO_3)_n$] particles were attached on the surface of BCP, which facilitated the precipitation of Pb(II) to form $[Pb(PO_3)_2]_n$, $Pb_5(PO_4)_3OH$ and $PbHPO_4$. This study thus demonstrated the effect of pyrolysis temperature on the enhancing removal capability of P-modified biochar for Pb(II) from aqueous solutions.

Keywords: Biomass co-pyrolysis; Modified biochar; Heavy metal removal; Adsorption mechanisms; Wastewater treatment

1. Introduction

Lead (Pb) is one of the most widely used heavy metals with consumption reaching about 11.89 million tons in 2019 (www.ilzsg.org). Pb can be discharged into the aquatic environment from a wide range of sources such as lead-acid battery manufacture, electroplating industry, paint, and pipe and gasoline industries [1]. Since Pb is highly toxic and non-biodegradable, it can accumulate in human body through the water and food chains, posing serious threat to human health even at trace concentrations [2]. Therefore, it is necessary to seek approaches that can efficiently and selectively remove Pb from aquatic environment in simple steps.

Many technologies, such as precipitation, coagulation, membrane filtration, ion exchange, bioremediation, and adsorption, have been utilized to remove heavy metals from aquatic environment [3]. Among them, adsorption has been regarded as one of the most promising technology because of its low cost, high efficiency, simple operation, and environmental friendliness. A series of adsorbents, such as nanomaterials [4], copolymers [5], and activated

carbon [6], have been developed to remove Pb. However, the practical application of these materials in large-scale wastewater treatment is limited by the potential risk of secondary pollution, high cost, and/or complex production procedures. Biochar, a carbonaceous product derived from thermal conversion of carbon-rich biomass in an oxygen-limited environment, has gained enormous attention in the removal of pollutants because it is an effective, cheap, and renewable material [7]. However, in current researches, biochar was found to have a limited ability to adsorb high levels of contaminants including Pb [8, 9]. The adsorption capacity of biochar is directly related with its physico-chemical properties, such as surface area, functional groups and cation exchange capacity [10]. Thus, extensive attention has recently been paid to improve its properties in order to enhance the adsorption capacity for specific pollutant.

The properties of biochar mainly depend on feedstock types and pyrolysis conditions, i.e., temperature, residence time, heating rate, and reactor type (slow pyrolysis, fast pyrolysis, hydrothermal carbonization and gasification) [11]. Considerable attention has been paid to optimize the pyrolysis conditions to improve the properties of biochar [12, 13]. Moreover, various modification methods, including chemical modification (with acid, alkali, oxidizing agent, metal salts), and physical modification (with steam, gas purging, ball milling), have been applied to improve biochar's performance in environmental remediation [14, 15].

Modification of biochar with phosphorous (P) material may be a promising way to remove Pb from water. Most researches focused on the HPO_3 modification of biochar to improve heavy metal adsorption performances in aqueous systems [16-18]. Few studies also showed that biochar modified with inorganic P salts such as Na_2HPO_4 [19], KH_2PO_4 and CaH_2PO_4 [20] could increase its heavy metal adsorption capacity. For instance, Gao et al. (2019) [20] illustrated that KH_2PO_4 was transformed into $(KPO_3)_n$ and $K_4P_2O_7$ during co-pyrolysis of rape straw with KH_2PO_4 (w/w, 20%) at 500 °C, which complexed with Pb(II), resulting in about 8-fold increase of Pb(II) removal capacity compared to the pristine biochar. The preparation/modification conditions,

especially temperature, could play a significant role in the properties of polyphosphates, such as crystallinity, chain length and solubility [21, 22], which would affect their capabilities to complex metals [23, 24]. Hence, it is essential to understand the influence of pyrolysis temperature on the physico-chemical characteristics and Pb(II) adsorption performance of dihydric phosphate-modified biochar.

In this study, a P-modified biochar was produced by the pyrolysis of the KH_2PO_4 pre-impregnated poplar sawdust at 300, 500, and 700 °C. The objectives are to: (1) investigate the influence of pyrolysis temperature on the physico-chemical, morphological and spectroscopic properties of KH_2PO_4-modified biochar, (2) determine the adsorption capacity of Pb(II) by KH_2PO_4-modified biochar from aqueous solution, and (3) explore the removal mechanisms of Pb(II) by KH_2PO_4-modified biochar.

2. Materials and methods

2.1 Biochar preparation

All chemicals used in this study were of analytical grade. Lead nitrate ($Pb(NO_3)_2$), potassium dihydrogen phosphate (KH_2PO_4), ferric nitrate ($Fe(NO_3)_3$), copper nitrate ($Cu(NO_3)_2$), sodium chloride (NaCl), nitric acid (HNO_3), and sodium hydroxide (NaOH) were purchased from Sinopharm Chemical Reagent Co. Ltd, Shanghai, China.

Poplar (*Populus euramericana* cv) sawdust was collected from a timber processing plant in Huai'an City, China. Table S1 showed the characteristics of poplar sawdust, including lignocellulosic composition, ultimate and proximate analyses. The feedstock was first air-dried, and then passed through a 60 mesh sieve. About 50.0 g sawdust was impregnated with a 250 mL of KH_2PO_4 solution (0.147 mol L^{-1}) with a mass ratio of 10:1 of precursor to KH_2PO_4. The mixture was agitated on a magnetic stirrer for 1h and placed at room temperature for 24 h, and then dried in oven at 110 °C for 8 h. About 5.0 g raw and impregnated samples were taken into a 50 mL porcelain crucible and thermally treated in a tube furnace under pure N_2 atmosphere

(99.999%, 200 mL min^{-1}) by raising to the desired temperatures (300, 500, and 700 °C) at a rate of 10 °C min^{-1}, and maintained for 2 h. All biochars were repeatedly washed with about 500 mL deionized water by suction filtration, and then dried in an oven at 110 °C for 8 h. Finally, all biochars were passed through a 100-mesh nylon sieve (149 μm). The obtained pristine biochar and KH_2PO_4-modified biochar were named BCX00 and BCPX00, respectively, in which X00 represented the pyrolysis temperature. Moreover, KH_2PO_4 was also pyrolyzed according to the same condition of biochar production.

2.2 Characterization of samples

The pH values of biochars were measured with a pH meter (PSH300, Sanxin, China) in a suspension of 0.5 g biochar in 5 mL deionized water. The point of zero charge (pH_{PZC}) value was measured using the method of pH shift [25]. Briefly, 30.0 mg samples were added to tubes with 10 mL solutions of 0.01 mol L^{-1} NaCl, which were adjusted to pH values of 2 to 8 ($pH_{initial}$), and shaken at 250 rpm at 25 °C. After 48 h, the pH_{final} of samples were measured and plotted against $pH_{initial}$. pH_{PZC} is the intersection point of the resulting curve with the line passing origin ($pH_{final} = pH_{initial}$). The carbon (C), hydrogen (H), nitrogen (N), and oxygen (O) contents were conducted using an elemental analyzer (Vario EL, Elementar, Germany). The ash contents of samples were determined using the standard GB/T 12496.3-1999 method [26].

Residual carbon in biochar was calculated based on biochar yield and total carbon content (Eq. 1):

$$\text{Residual carbon (\%)} = \left(\frac{C_{biochar}}{C_{biomass}}\right) * Y_{biochar} \quad (1)$$

where, $C_{biochar}$ and $C_{biomass}$ are total carbon contents (%) of the biochar and poplar sawdust, respectively, and $Y_{biochar}$ is the yield (%) of biochar.

Surface area and pore properties of biochars were determined using results of N_2 adsorption at 77 K using the Brunauer–Emmett–Teller (BET) method (ASAP 2020, Micromeritics, USA). Surface morphology of the samples was analyzed by scanning electron microscope coupled

with energy-dispersive X-ray spectrometry (SEM-EDS) (FEI Inspect S50, USA). Fourier transform infrared (FTIR) spectra of samples were recorded on a Nicolet iS50 spectrometer (Thermo Fisher Scientific, USA) in the region of 4000–400 cm^{-1}. X-ray diffraction (XRD) patterns were obtained using a powder X-ray diffractometer (PANalytical X'Pert3 Powder diffractometer, The Netherlands) equipped with Cu Kα radiation (λ = 0.154 nm) in the 2θ range of 10–80° at 40 kV and 40 mA.

2.3 Adsorption experiments

A stock solution (1200 mg L^{-1}) of Pb(II) was obtained by dissolving $Pb(NO_3)_2$ in deionized water. The isotherm adsorption experiments were conducted in 50 mL polypropylene centrifuge tubes containing 0.05 g biochar and 20 mL solution of varied Pb(II) concentrations (25−1200 mg L^{-1}) at pH= 5.0. The kinetic adsorption experiments were performed at different contact times (0.5 to 48 h) at an initial Pb(II) concentration of 400 mg L^{-1} at pH 5.0. To examine the effect of pH on adsorption, the initial pH value of mixture was adjusted to 2.0, 3.0, 4.0, 5.0, 6.0, and 7.0 ± 0.1 using 0.1 M or 0.01 M HNO_3 and NaOH.

Various metal ions existed in wastewater, which may affect Pb(II) adsorption on biochar. Na^+, Cu^{2+}, and Fe^{3+} are chosen as coexisting ions with different valence states. Competitive adsorption tests were conducted in binary-metal systems with varied Na^+, Cu^{2+}, and Fe^{3+}concentrations (0.5-20 mmol L^{-1}) and a constant Pb^{2+} concentration (1 mmol L^{-1}). All reaction mixtures were shaken in a rotary shaker at 150 rpm at 25 °C for 24 h (except the time varied in kinetic tests). The supernatants were filtered through a 0.45 μm membrane filter, and Pb, K, P, and other metals (Na^+, Cu^{2+}, and Fe^{3+}) concentrations in filtrates were measured using an inductively coupled plasma-optical emission spectrometer (ICP-OES, Optima 2000DV, Perkin Elmer, USA). All experiments were conducted in triplicate, and average values were reported. Residual solids were collected and dried at 110 °C, and were analyzed through FTIR, SEM-EDS and XRD to explore the adsorption mechanisms of Pb(II) on biochar.

The adsorption capacity of Pb(II) (Q_e, mg g^{-1}) was calculated using Eq. 2:

$$Q_e = V*(C_i - C_e)/M \quad (2)$$

where, C_i and C_e are the initial and final Pb(II) concentrations in solution (mg L^{-1}), V is the solution volume (L), and M is the biochar mass (g).

Kinetics and isotherms models are provided in Supplementary Material. Adsorption experiments were carried out in triplicates. Experimental data were the mean values for triplicate tests.

3. Results and discussion

3.1 Thermogravimetric analysis

The TG and DTG curves of poplar sawdust, KH_2PO_4 and mixture are shown in Fig. S1. Approximately 22.5, 33.7, and 86.0 wt% of poplar sawdust, KH_2PO_4 and mixture remained after pyrolysis at 800 °C. The mass loss of sawdust could be divided into two main stages: 95-150 °C and 240–370 °C, which were caused by the loss of water and decomposition of organic components (Fig. S1a). The three loss peaks of KH_2PO_4 were recorded at 220°C, 270°C and 320 °C, which attributed to the phase transition, partial and eventual decomposition of KH_2PO_4, respectively [27] (Fig. S1b). In comparison to single sawdust, the second loss peak of mixture shifted backward (from 350 °C to 330 °C).

3.2 Characterization of biochars

3.2.1 Physico-chemical properties

The yields of pristine biochars (BC) gradually decreased from 43.93 to 23.57% as the temperature increased from 300 °C to 700 °C (Table 1). The yields of KH_2PO_4-modified biochars (BCP) were much higher than those of BC, and BCP contained higher ash contents (18.97−32.81%) than BC (7.90−21.5%), due to the input of KH_2PO_4. The BC presented neutral reactions (pH=6.53-7.67), whereas BCP showed slightly lower pH values (pH=6.05-7.21) than BC (Table 1), which likely resulted from the acidity of KH_2PO_4 or its thermal alteration [28].

The pH_{pzc} values of BCP (4.68, 5.02 and 5.16 for BCP300, BCP500, and BCP700, respectively) were lower than those of BC (5.21, 5.28 and 5.61 for BC300, BC500, and BC700, respectively) (Table 1), indicating that the introduction of KH_2PO_4 reduced the positive surface charge of biochar. Moreover, lower pH_{pzc} values of BCP indicated more stability and higher dispersibility in solution [20].

With increasing pyrolysis temperature from 300 °C to 700 °C, C content of BC increased from 73.9% to 89.1%, whereas H and O contents decreased from 2.04% to 0.94%, and from 20.2% to 5.89%, respectively (Table 1). Although C content of BCP (63.0−76.1%) was less than that of BC, the addition of KH_2PO_4 increased the residual carbon content or carbon retention (Eq. 1). The higher the pyrolysis temperature, the more carbon was retained (Table 1), which agreed with previous reports where co-pyrolysis of biomass and P-salts, e.g., $Ca(H_2PO_4)_2$, increased carbon retention in biochar [29-31]. The H/C ratio was lower in BCP than that in BC (Table 1), suggesting an enhanced aromatic structure in BCP [20]. Expectedly, KH_2PO_4 addition increased the P content from 0.10−0.15% in BC to 4.14−6.78% in BCP, and the O content was also relatively high (9.0-25.7%) in BCP than BC (5.9-20.2%) (Table 1).

Table 1 Physico-chemical properties of biochars

	pH	pH_{zpc}	Yield (%)	Ash (%)	C (%)	RC (%)	H (%)	N (%)	O (%)	P (%)	H/C
PS	-	-	-	3.31 ±0.05	51.4 ±0.6	-	3.69 ±0.04	0.74 ±0.01	30.2 ±0.4	0.07 ±0.00	0.86 ±0.02
BC300	6.53 ±0.07	5.21 ±0.02	43.9 ±0.8	7.90 ±0.11	73.9 ±0.9	64.4 ±0.6	2.04 ±0.03	0.54 ±0.01	20.2 ±0.5	0.10 ±0.00	0.33 ±0.01
BCP300	6.05 ±0.06	4.68 ±0.01	53.6 ±0.7	19.0 ±0.18	63.0 ±0.8	67.0 ±0.6	1.53 ±0.01	0.33 ±0.00	26.6 ±0.2	4.14 ±0.02	0.29 ±0.02
BC500	6.94 ±0.06	5.38 ±0.04	27.0 ±0.6	16.8 ±0.26	84.6 ±1.1	45.3 ±0.5	1.48 ±0.01	0.32 ±0.00	10.6 ±0.2	0.13 ±0.00	0.21 ±0.01
BCP500	6.51 ±0.07	5.02 ±0.03	37.5 ±0.4	25.6 ±0.25	71.0 ±0.8	52.8 ±0.4	1.09 ±0.01	0.20 ±0.00	15.1 ±0.2	5.94 ±0.05	0.18 ±0.00
BC700	7.67 ±0.08	5.61 ±0.05	23.6 ±0.4	21.5 ±0.29	89.1 ±1.0	41.7 ±0.5	0.94 ±0.02	0.19 ±0.01	5.89 ±0.07	0.15 ±0.01	0.13 ±0.01
BCP700	7.21 ±0.08	5.16 ±0.02	34.1 ±0.6	32.8 ±0.33	76.1 ±0.7	51.5 ±0.3	0.56 ±0.01	0.11 ±0.00	9.01 ±0.06	6.78 ±0.08	0.09 ±0.00

PS: Poplar sawdust; RC: Residual carbon

3.1.2 SEM-EDS analysis

The characteristic fibrous structure of the poplar sawdust biomass was still conserved in BC, and the surface of BC was generally smooth in appearance (Fig. 1). The KH_2PO_4 modification seemed to have no obvious influence on the morphology of biochars, but the surface of biochars became coarse (Fig. 1). Many irregular particles were uniformly dispersed on the BCP surfaces, and the size of particles increased with the increase in pyrolysis temperature. Moreover, the EDS result showed that compared with BC, high K, P, and O contents was found in BCP (Fig. 1), suggesting that KH_2PO_4 or its pyrolysis production loaded in BCP.

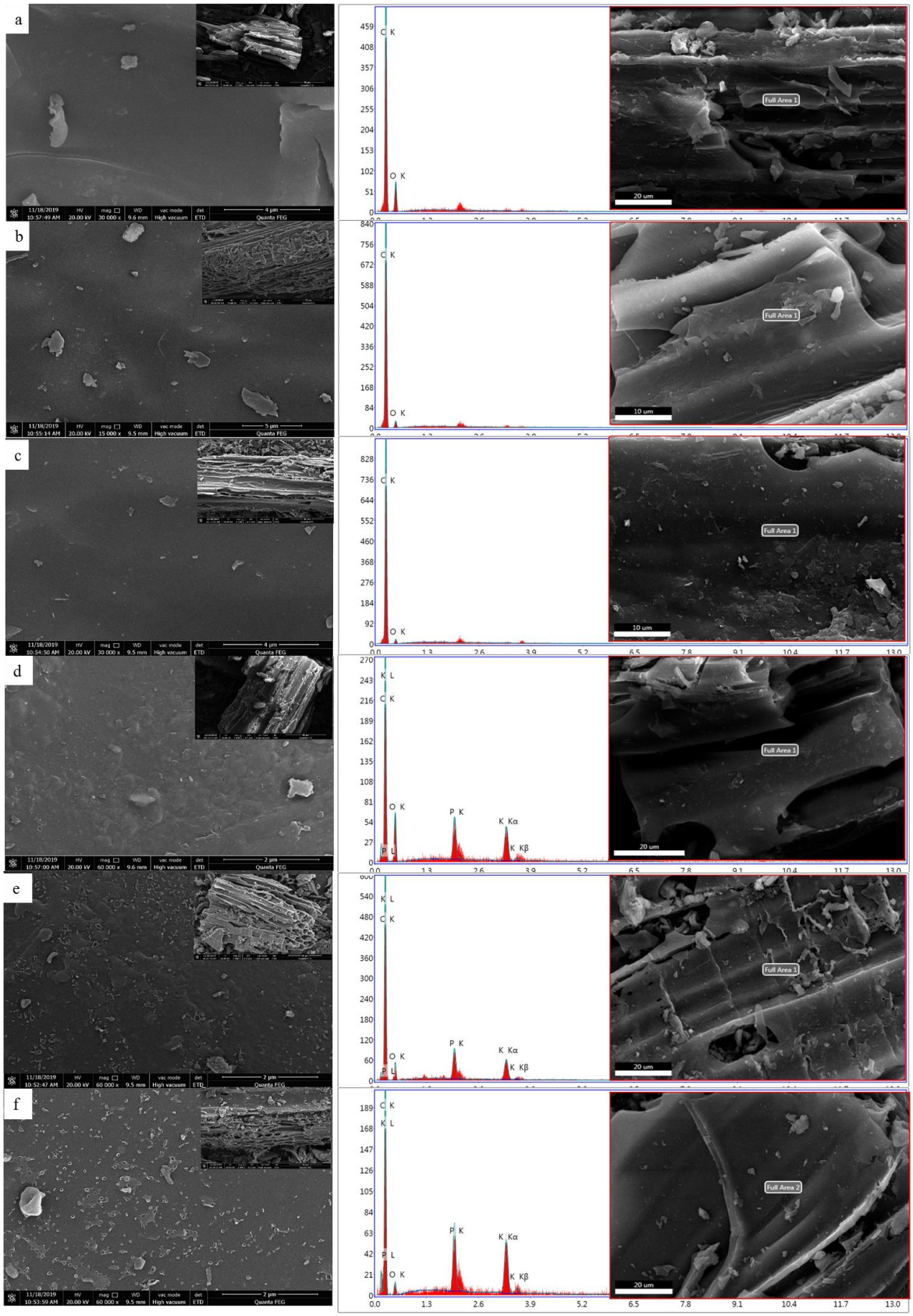

Fig. 1 SEM images of BC300 (a), BC500 (b), BC700 (c), BCP300 (d), BCP500 (e) and BCP700 (f)

3.1.3 FTIR analysis

With increasing pyrolysis temperature, the band intensities representing OH (3420 cm^{-1}), C-H (2934 cm^{-1}), COOH (1698 cm^{-1}) and aromatic C=O or C=C (1604 cm^{-1}) [32] decreased markedly or almost disappeared (Fig. 2), which are consistent with those reported in earlier studies [33, 34]. The band at about 1030 cm^{-1} associated with the C-O stretching vibration of aromatic ring became stronger with the increasing temperature [35]. Furthermore, a marked shift of bands from 1453 to 1422 cm^{-1} revealed an increasing carbonate ($CaCO_3$) content in BCP with rising pyrolysis temperature [36].

After KH_2PO_4 modification, some additional bands at 1274, 1150 and 499 cm^{-1} were observed (Fig. 2). In addition to the newly appeared bands, an increase in intensities of bands at about 1100, 860, 763, 679 and 603 cm^{-1} were observed in BCP (Fig. 2). These changed bands were also visible on the FTIR spectra of the thermally treated KH_2PO_4 samples (Fig. S2). The band at 1273 cm^{-1} originated from the asymmetrical stretching vibrations of O-P-O, while those at 1150, 763 and 679 cm^{-1} were attributed to the symmetric stretching vibrations of O-P-O [37]. The bands around 1100 and 860 cm^{-1} were assigned to the symmetric stretching vibrations of PO_3 groups [38]. Two bands at 603 and 499 cm^{-1} were assigned to the bending vibrations of O-P-O [39]. Furthermore, compared with the bands related to PO_3 groups in the thermally treated KH_2PO_4 (1108 and 1117 cm^{-1}), lower wavenumber bands at 1101 and 1098 cm^{-1} were observed in BCP500 and BCP700, respectively (Fig. 2), which were likely attributed to the stretching vibrations of C-O-P [30]. The formation of C-O-P would block active carbon sites to reduce carbon loss in BCP, which could also explain the increased carbon retention in BCP [30].

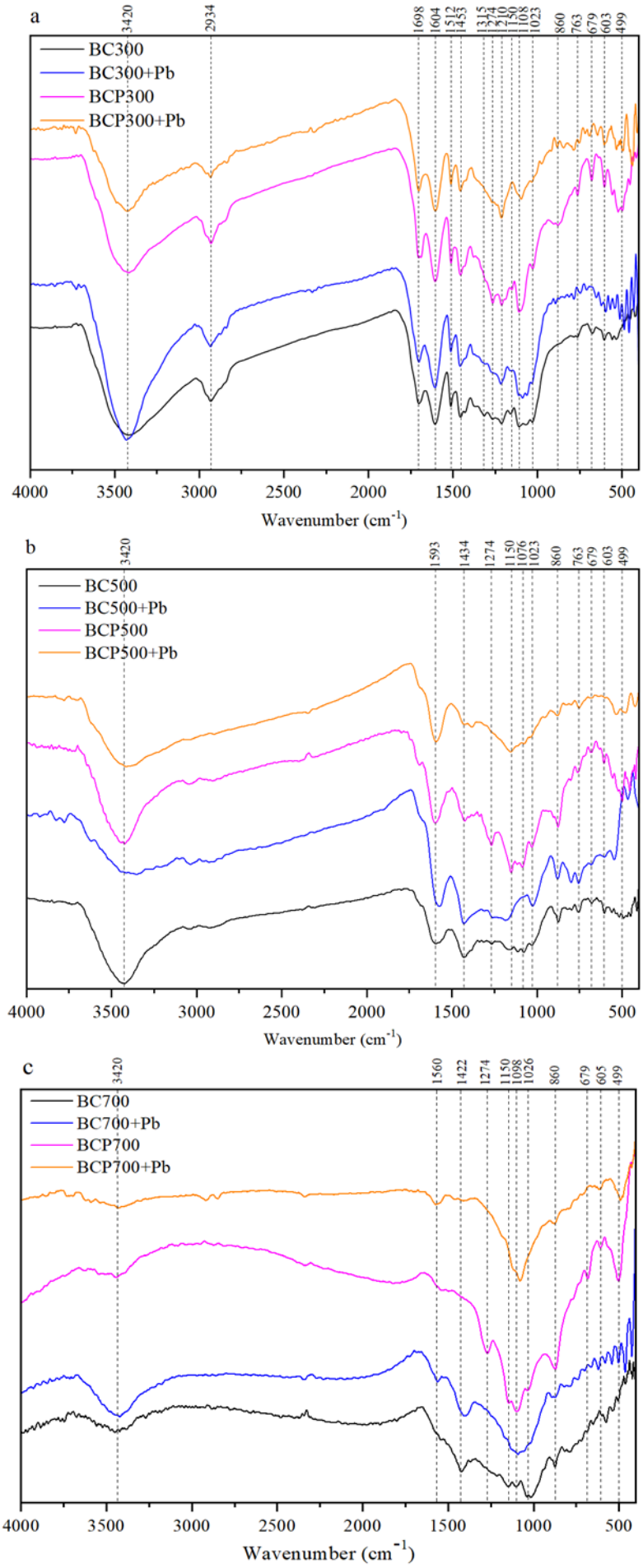
a
3420
2934
1698
1604
1512
1453
1315
1274
1210
1150
1108
1023
860
763
679
603
499
BC300
BC300+Pb
BCP300
BCP300+Pb
4000
3500
3000
2500
2000
1500
1000
500
Wavenumber (cm-1)
b
3420
1593
1434
1274
1150
1076
1023
860
763
679
603
499
BC500
BC500+Pb
BCP500
BCP500+Pb
4000
3500
3000
2500
2000
1500
1000
500
Wavenumber (cm-1)
c
3420
1560
1422
1274
1150
1098
1026
860
679
605
499
BC700
BC700+Pb
BCP700
BCP700+Pb
4000
3500
3000
2500
2000
1500
1000
500
Wavenumber (cm-1)

Fig. 2 FTIR spectra of BC300 and BCP300 (a), BC500 and BCP500 (b), BC700 and BCP700 (c) before and after Pb(II) adsorption

3.1.4 XRD analysis

All pristine BC showed diffraction peaks of SiO_2 (2θ = 20.9 º, 26.6º and 50.2º, JCPDS#01-089-1961) and $CaCO_3$ (2θ = 29.5º, JCPDS#00-005-0586), whereas BC300 also showed CaC_2O_4 (2θ = 14.9 º and 20.8 º, JCPDS#00-003-0090) peaks (Fig. 3). BC700 showed stronger diffraction peaks of $CaCO_3$ than BC300 and BC500, which was consistent with FTIR results (Fig. 2). Compared with BC, a stronger reflection at 2θ=26.6º was observed in BCP500 and BCP700, which could be attributed to the formation of C-P or C-O-P groups [28]. New reflections of $(KPO_3)_n$ (2θ = 19.6°, 26.3°, 25.9°, 27.8° and 35.6°, JCPDS#00-035-0819) were observed in BCP (Fig. 3), implying that KH_2PO_4 was transformed into $(KPO_3)_n$ at ⩾300 °C. These results agreed with those obtained by Lee (1996) [22] and Shenoy et al. (2010) [40], who concluded that the formation of various monoclinic $(KPO_3)_n$ occurred at through the dehydration and condensation of KH_2PO_4 ($nKH_2PO_4 \rightarrow K_nH_2P_nO_{3n+1} + (n-1)H_2O$) above 258 °C (Fig. S3). Besides, BCP showed reflections (2θ = 17.5°, 23.9° and 30.7°, JCPDS#01-072-1021) attributed to KH_2PO_4 (Fig. 3), which might have been derived from the hydrolysis of $(KPO_3)_n$ during the water washing process of BCP. Reflections (2θ = 29.9° and 31.6°, JCPDS#00-022-0805) corresponding to $K_2CaP_2O_7$ appeared only in BCP700 (Fig. 3), which was likely formed by the reaction between $CaCO_3$ and KH_2PO_4 ($2KH_2PO_4 + CaCO_3 = K_2CaP_2O_7 + 2H_2O + CO_2$) [41].

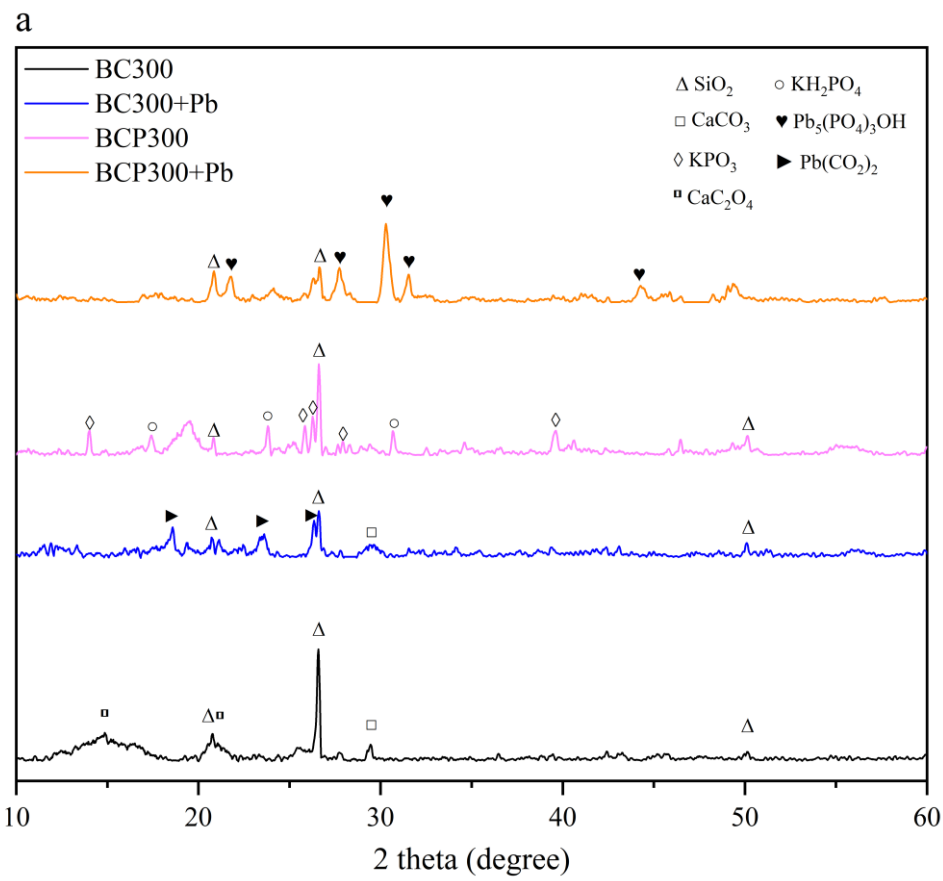
a
BC300
BC300+Pb
BCP300
BCP300+Pb
Δ SiO2
○ KH2PO4
□ CaCO3
♥ Pb5(PO4)3OH
◊ KPO3
▶ Pb(CO2)2
▫ CaC2O4
10
20
30
40
50
60
2 theta (degree)

247

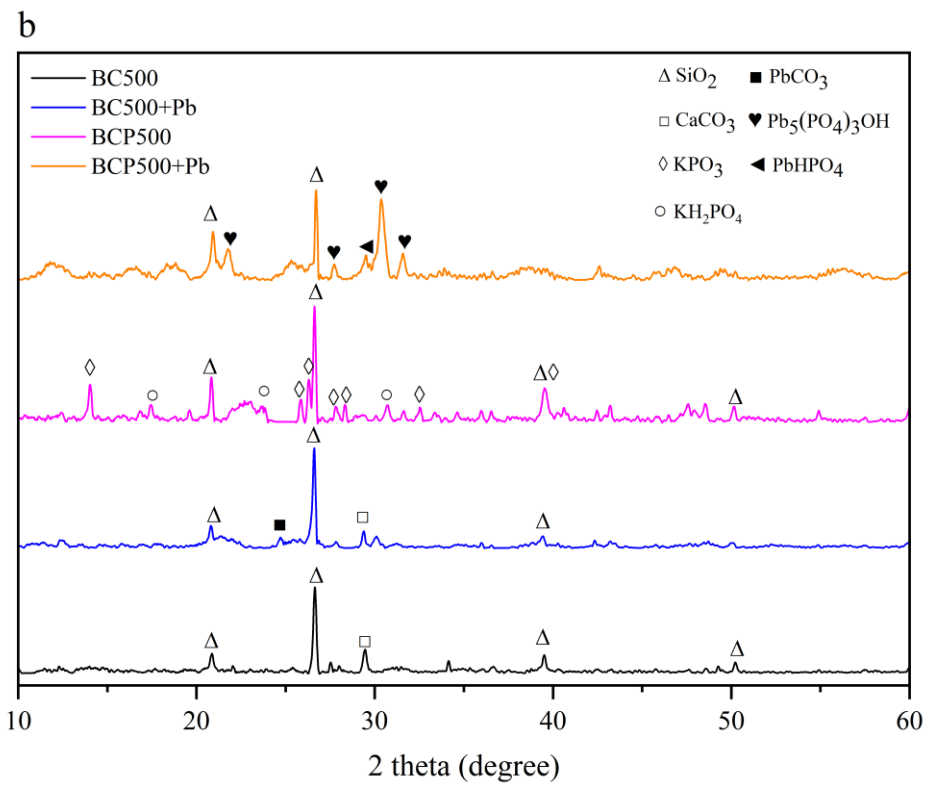
b
BC500
BC500+Pb
BCP500
BCP500+Pb
Δ SiO2
■ PbCO3
□ CaCO3
♥ Pb5(PO4)3OH
◊ KPO3
◀ PbHPO4
○ KH2PO4
10
20
30
40
50
60
2 theta (degree)

248

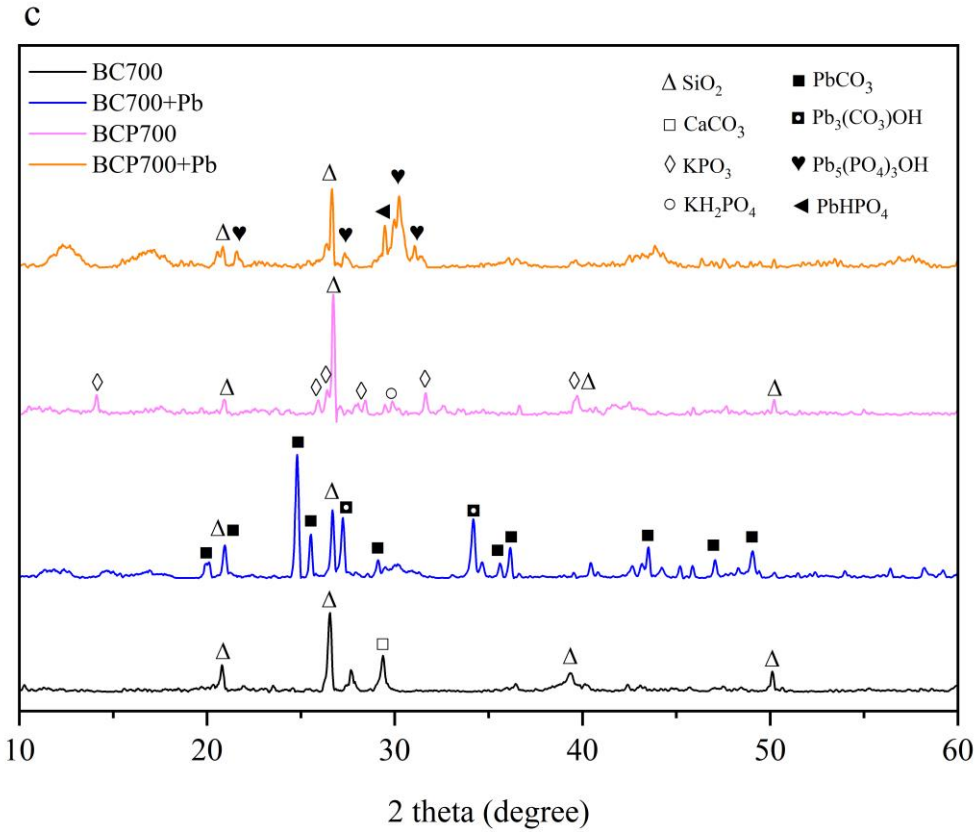

Fig. 3 XRD patterns of BC300 and BCP300 (a), BC500 and BCP500 (b), BC700 and BCP700 (c) before and after Pd(II) adsorption

3.1.5 Surface area and pore characteristics

When the temperature increased from 300 °C to 700 °C, the specific surface area (SSA) of BC increased from 3.01 to 303.45 $m^2\ g^{-1}$, and the total pore volume increased from 0.006 to 0.182 $cm^3 \cdot g^{-1}$ (Table S2). The formation of SSA during pyrolysis is mainly associated with volatilization processes and the loss of organic compounds, which creates voids within the biochar matrix [42]. Therefore, the higher temperature, the lager SSA and pore volume. The micropore volume of BC increased notably with rising pyrolysis temperature (Table S2). The micropore volume of BCP700 comprised approximately two-thirds of the total pore volume. The KH_2PO_4 modification reduced the surface area and pore volume of biochars (Table S2). This was probably because the formation of C-O-P/C-P in BCP could decrease the release of

volatile matter, thus reducing the generation of voids within the biochar matrix [43]. Furthermore, many $(KPO_3)_n$ particles distributed on the surface of BCP could clog the pores of BCP, thereby resulting in a smaller pore volume. Similar results were observed in γ-Fe_2O_3-loaded biochar where the γ-Fe_2O_3 blocked the pores of the biochar [44].

3.2. Adsorption of Pb(II)

3.2.1 Effect of pH

The initial solution pH significantly influenced the adsorption capacities of Pb(II) on both BC and BCP (Fig. 4). The adsorption capacities of BC and BCP increased sharply with increasing pH value from 2.0 to 3.0, and then gradually increased with increasing pH from 3.0 to 7.0, attaining the highest adsorption capacity at pH=7.0 (removal efficiency≈100%). At low pH, a large amount of H^+ ions competed with Pb(II) cations for the adsorption sites on biochars, and an electrostatic repulsion also prevailed between Pb(II) ions and the positively charged biochar surface [45], which led to low adsorption capacities. With the increase of pH, the positive charge of biochar surface became less, and finally changed to a negative charge at high pH, which likely enhanced the electrostatic attraction of Pb(II) ions and negatively charged biochar surface [46]. Above pH 6.0, the predominant species of Pb(II) would be precipitated $Pb(OH)_2$ [47], which might also be responsible for the increased adsorption capacities of Pb(II) at pH 6.0–7.0. The equilibrium solution pH values of all biochars were below 6.0 only under the condition of initial solution pH ≤5.0 (Fig. 4). In order to avoid the formation of $Pb(OH)_2$, pH 5.0 was selected as the optimum pH for adsorption kinetic and isotherm experiments.

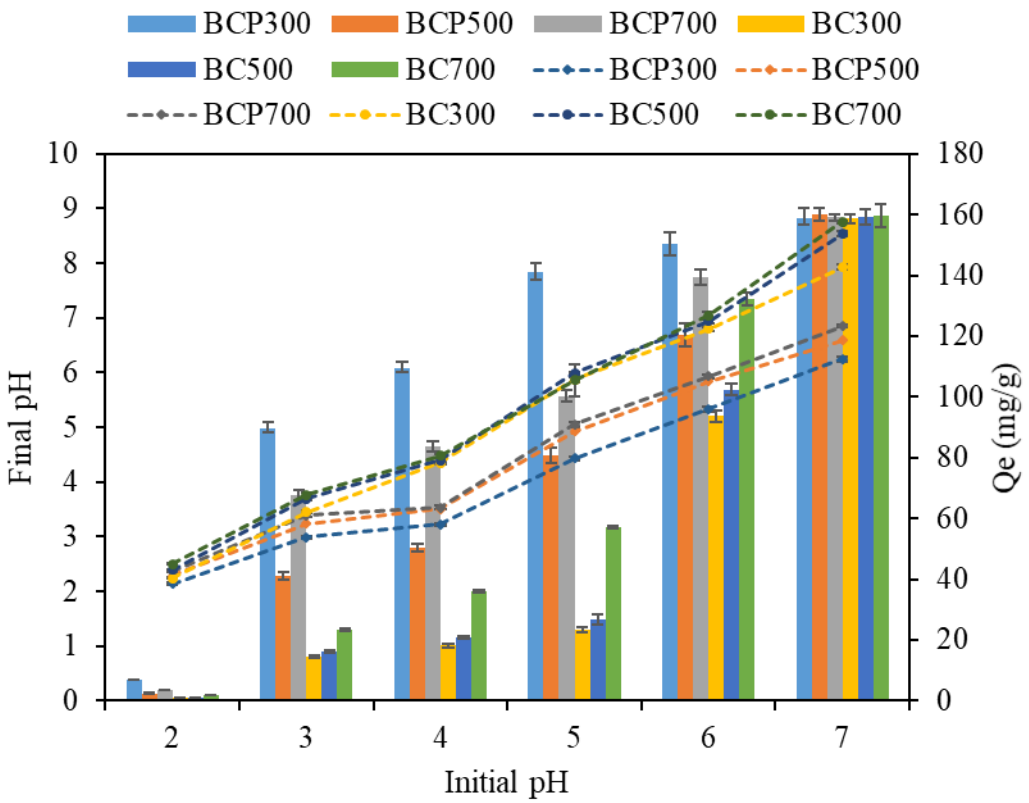

Fig. 4 Effect of initial pH on the adsorption capacities of Pb(II) by biochars (dash line and bar graph indicated the final pH and adsorption capacity of Pb(II), respectively.)

3.2.2 Adsorption kinetics

The adsorption of Pb(II) onto BC and BCP showed two distinct phases: a rapid initial phase over the first 4 h, and then a slow adsorption phase to reach equilibrium (Fig. 5). No obvious effect of pyrolysis temperature on the equilibrium time was observed in this study. Similar result was reported by other researchers [48, 49]. The experimental data of Pb(II) adsorption onto all biochars fitted better to the pseudo-second-order (PSO) than pseudo-first-order (PFO) model, according to the R^2 and χ^2 values (Table 2), indicating that the Pb(II) adsorption process was mainly controlled by chemical interactions [50]. The Pb(II) adsorption capacities calculated from the PSO model (Q_e = 142.26, 81.75, and 107.70 mg g^{-1} for BCP300, BCP500, and BCP700, respectively) onto BCP were higher than those of BC (Q_e = 23.76, 27.07, and 61.99 mg g^{-1} for

BC300, BC500, and BC700, respectively), implying that KH_2PO_4 modification improved the Pb(II) adsorption performance of biochar. Furthermore, the initial adsorption rate (v_0) of BC increased as the pyrolytic temperature increased, indicating that the complexation of Pb(II) ions with oxygen-containing functional groups did not contribute much to the adsorption of Pb(II) on biochar. Xu et al. (2014) also found that the contribution of complexation of Pb(II) with organic functional groups in manure and rice straw biochars was very low [51]. In contrast, the v_0 values of BCP were as follows: BCP300> BCP700>BCP500.

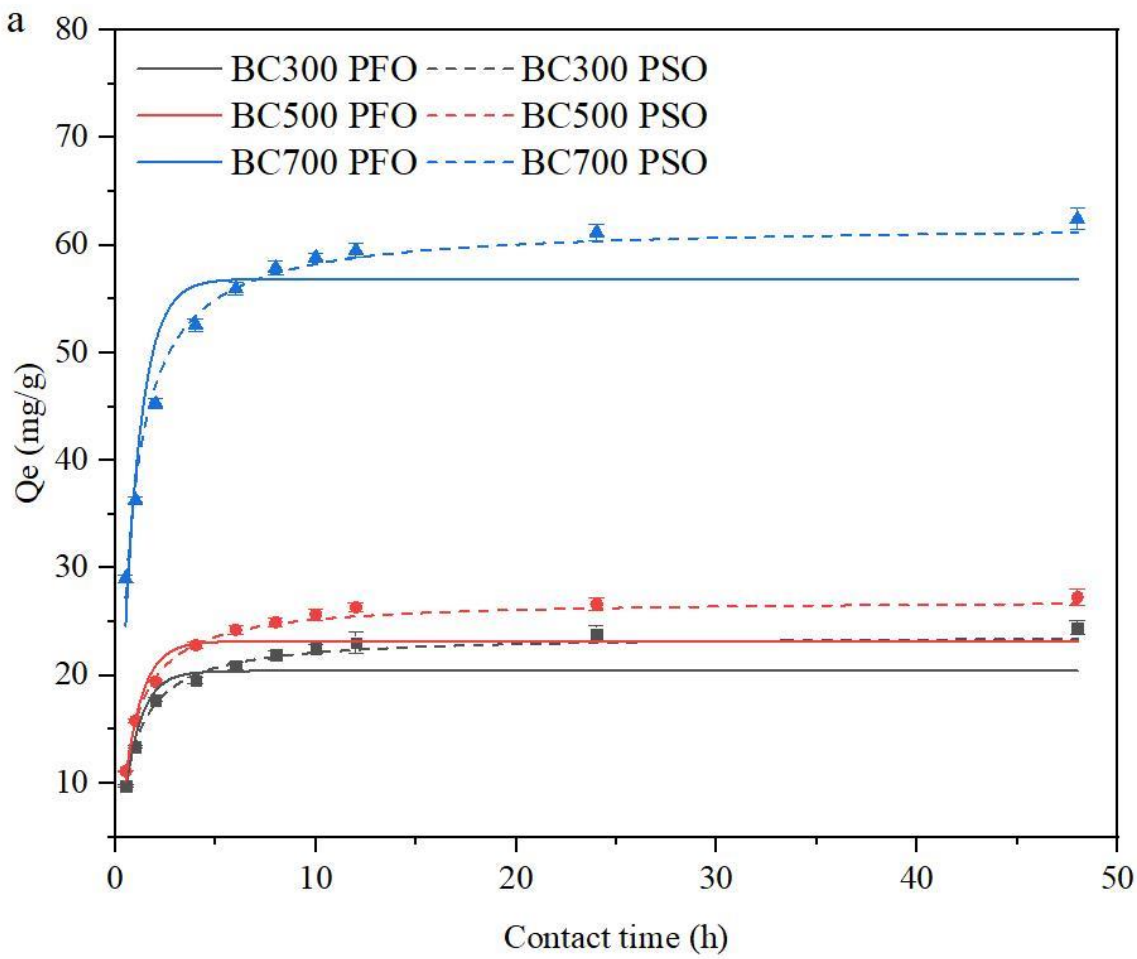

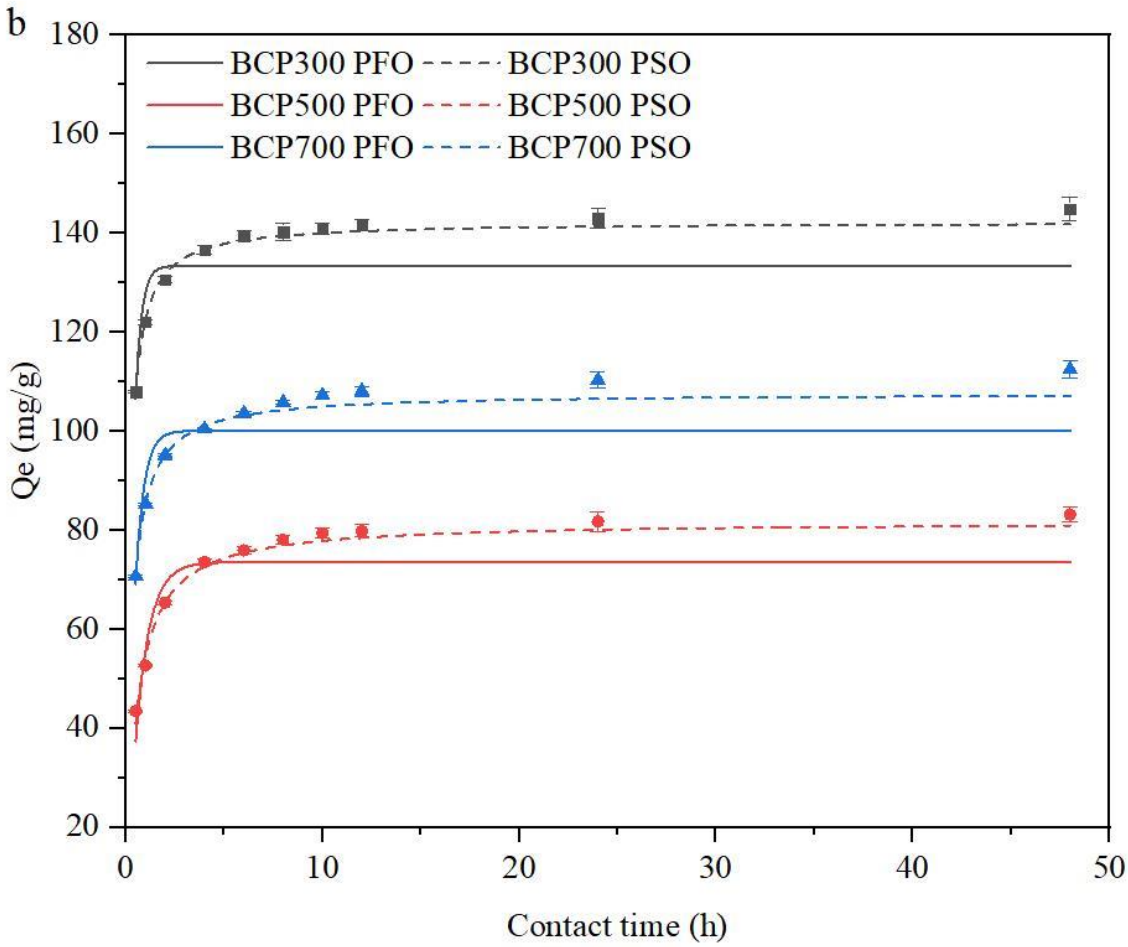

Fig. 5 Kinetics adsorption of Pb(II) on (a) BC, (b) BCP (biochar dosage 2.5 g L^{-1}, Pb(II) concentration = 400 mg L^{-1}, pH=5.0)

Table 2 Kinetic parameters for Pb(II) adsorption onto biochar

	pseudo–first order (PFO)				pseudo–second order (PSO)				
	Q_e (mg g^{-1})	k_1 (h^{-1})	R^2	χ^2	Q_e (mg g^{-1})	k_2 (g (mg h)$^{-1}$)	R^2	χ^2	v_0 (mg·g^{-1}·h^{-1})
BC300	20.4	1.21	0.947	3.88	23.8	0.057	0.995	1.87	32.29
BC500	23.2	1.16	0.929	2.98	27.1	0.050	0.996	0.59	36.72
BC700	56.9	1.14	0.917	5.74	62.0	0.025	0.988	1.93	96.10
BCP300	133	3.21	0.876	3.94	142	0.044	0.997	0.14	887.22
BCP500	73.5	1.42	0.870	4.94	81.8	0.024	0.991	0.40	160.59

BCP700	100	2.35	0.943	4.74	108	0.035	0.996	0.43	408.24

3.2.3 Adsorption isotherms

The adsorption isotherms of Pb(II) onto biochars were graphed in Fig. 6. The pyrolysis temperature had an obvious influence on the adsorption capacities of BC and BCP. The Pb(II) adsorption onto BC was better fitted to the Langmuir model than the Freundlich model (Table 3), indicating a monolayer type adsorption onto the homogenous sites of BC [52]. The Langmuir maximum adsorption capacities (q_{max}) of BC increased from 24.3 to 59.3 mg g^{-1} with the pyrolysis temperature increasing from 300 to 700 °C (Table 3). Unexpectedly, after KH_2PO_4 modification, the adsorption capacities of biochars to Pd(II) was decreased obviously when the Pb(II) concentration was low (⩽100 mg L^{-1}), whereas at high Pb(II) concentration (⩾200 mg L^{-1}), it was increased dramatically. Therefore, the adsorption isotherm data of ⩾200 mg L^{-1} Pb(II) onto BCP was simulated with both models. According to the correlation determination R^2 and chi-squared χ^2 (Table 2), adsorption of Pb(II) onto BCP300 was better fitted to the Langmuir model than the Freundlich model, whereas this was opposite for BCP500 and BCP700, implying the occurrence of heterogeneous multilayer adsorption of Pb(II) on the surface of BCP500 and BCP700 [53]. Also, the q_{max} value of BCP300 for Pb(II) (154.7 mg g^{-1}) was higher than those of BCP500 (92.4 mg g^{-1}) and BCP700 (95.2 mg g^{-1}). In addition, the calculated q_{max} of Pb(II) onto BCP300 was similar or even higher than those of other reported biochars (Table S3).

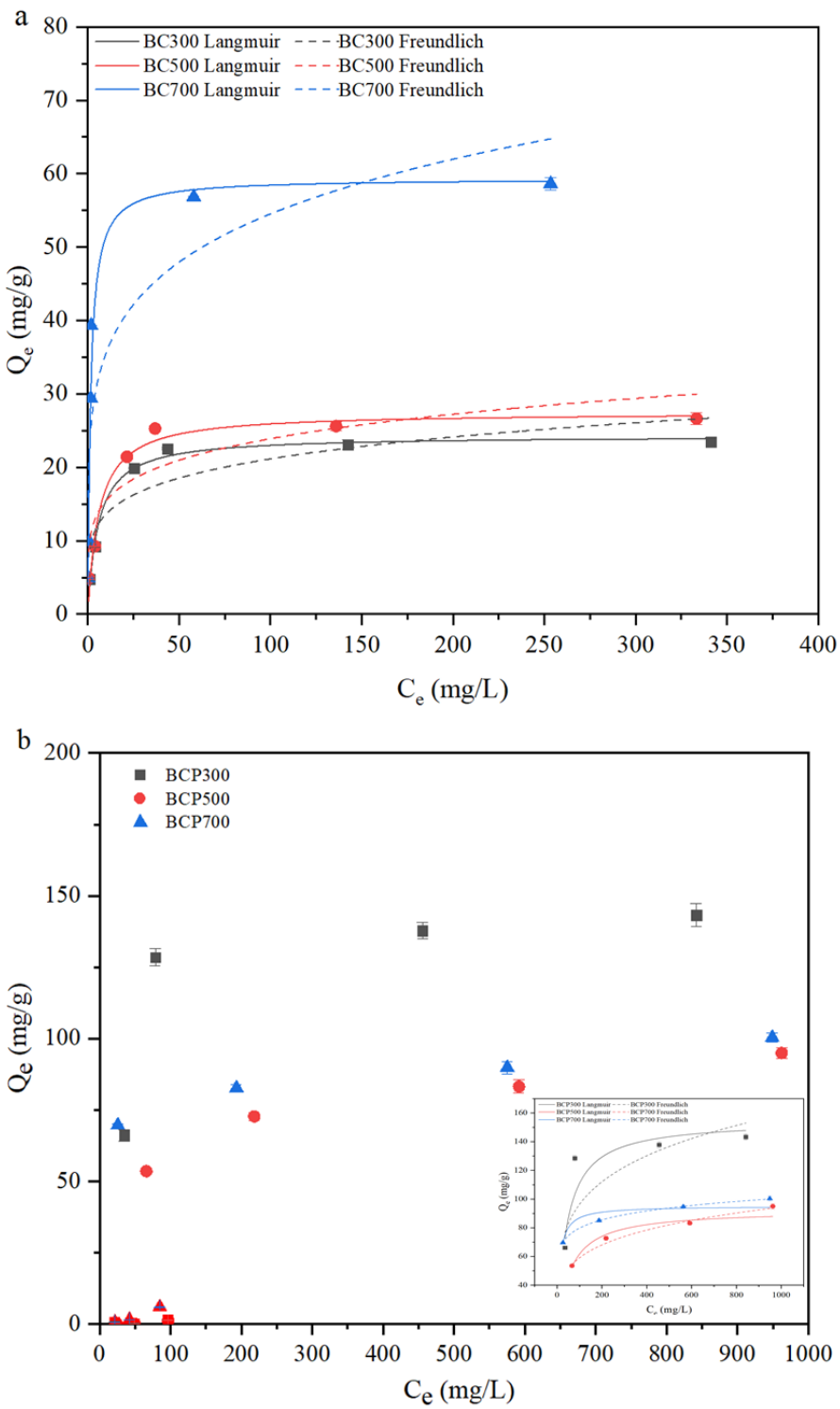

Fig. 6 Adsorption isotherms of Pb(II) on biochars (biochar dosage 2.5 g L^{-1}, pH=5.0)

Table 3 Isotherm parameters for Pb(II) adsorption onto biochar

	Langmuir	Freundlich

	q_{max} (mg g^{-1})	K_L (L mg^{-1})	R^2	χ^2	1/n	K_F	R^2	χ^2
BC300	24.3	0.177	0.991	0.36	0.190	8.81	0.799	4.68
BC500	27.5	0.167	0.966	1.12	0.188	10.0	0.818	5.97
BC700	59.3	0.661	0.946	2.09	0.185	23.3	0.784	21.66
BCP300	154.7	0.025	0.901	7.21	0.217	35.5	0.748	17.07
BCP500	92.4	0.020	0.965	0.72	0.204	23.2	0.985	0.22
BCP700	95.2	0.105	0.953	0.74	0.100	50.3	0.999	0.00

3.2.4 Effect of coexisting metals ions

To evaluate the ability of BCP300 to adsorb Pb(II) from aqueous solutions at different ionic strengths and coexisting metal ions, several experiments were performed at various concentrations of $NaNO_3$, $Fe(NO_3)_3$, and $Cu(NO_3)_3$. With increasing ionic strengths, except for 0.5 mmol L^{-1}, Na^+ had negligible effect on Pb(II) adsorption (Fig. 6), indicating that Na^+ did not compete with Pb(II) for the adsorption sites on BCP300 surface. Unlike Na^+, low concentration of Fe^{3+} and Cu^{2+} (0.5 mmol L^{-1}) promoted the adsorption capabilities of Pb(II), whereas further raising the concentration of Fe^{3+} and Cu^{2+} led to a gradually lowered adsorption (Fig. 6), suggesting that these cations competed with Pb(II) for the adsorption sites, and the effect was severe especially for high Fe^{3+} concentrations.

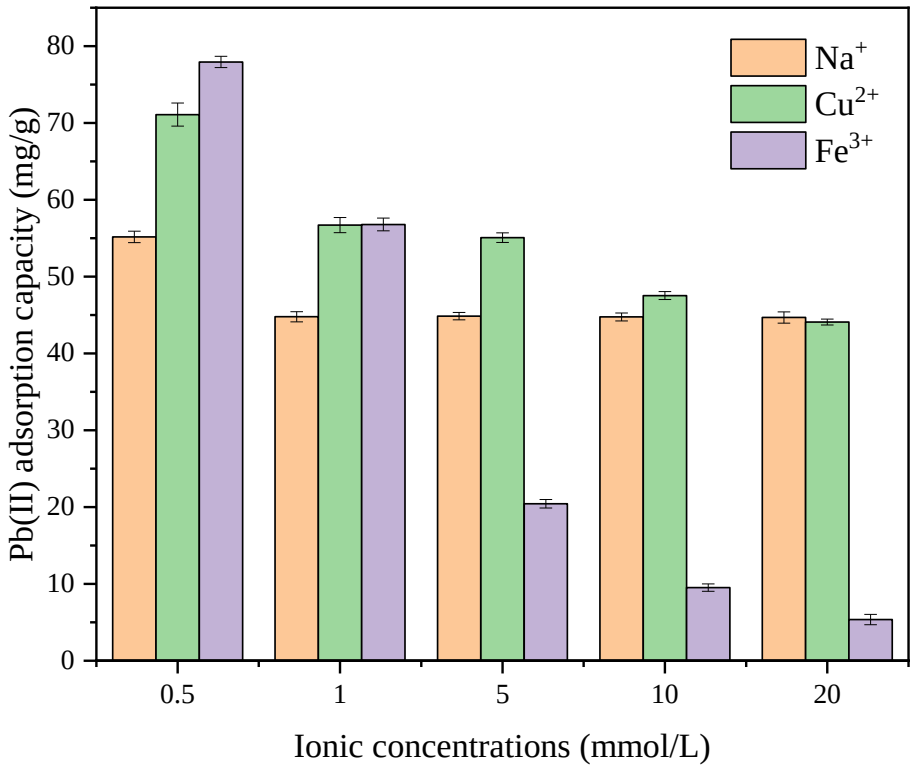

Fig. 6 Effect of coexisting metal ions (Na^+, Cu^{2+} and Fe^{3+}) on Pb(II) adsorption by BCP300 (biochar dosage 2.5 g L^{-1}, pH=5.0, initial concentration of Pb(II)=1 mmol L^{-1}, Q_e=67.0 mg g^{-1})

3.3. Mechanism of Pb(II) adsorption

3.3.1 Pb(II) adsorption on BC

The XRD patterns confirmed the presence of mineral $Pb(CO_2)_2$ (JCPDS#00-001-0285) in BC300+Pb, whereas the characteristic reflections of $PbCO_3$ (JCPDS#01-070-2052) appeared in BC500+Pb and BC700+Pb (Fig. 3), implying that Pb(II) ions were precipitated with carbonate. Notably, $2PbCO_3 \cdot Pb(OH)_2$ (JCPDS#00-013-0131) was observed in BC700+Pb, which was related to higher alkalinity of BC700 (pH=7.67) than remaining samples. The FTIR spectra of BC300 following Pb(II) adsorption did not notably change (Fig. 2). For BC500 and

BCP700, the band at 1593 cm^{-1} shifted appreciably to a lower wavelength (1570 and 1560 cm^{-1}, respectively) after Pb(II) adsorption, which indicated that Pb(II)-π interaction might also be responsible for the adsorption of Pb(II) on BC500 and BC700. Overall, the FTIR and XRD results indicated that mineral precipitation and cation–π interaction jointly contributed to Pb(II) adsorption on biochar produced at high temperature.

3.3.2 Pb(II) adsorption on BCP

After Pb(II) adsorption, the intensities of IR bands assigned to P-O-P, PO_3 or O-P-O groups in BCP reduced, or even disappeared (Fig. 2), revealing that these groups likely interacted with Pb(II). In addition, Pb orthophosphate precipitates ($Pb_5(PO_4)_3OH$ and $PbHPO_4$) were found in the XRD patterns of Pb(II)-loaded BCP (Fig. 3), which would result from the following reactions (Eq. 3 and 4):

$$Pb^{2+} + KH_2PO_4 \rightarrow PbHPO_4 + H^+ \quad (3)$$

$$5PbHPO_4 + H_2O \rightarrow Pb_5(PO_4)_3OH + 2H_2PO_4^- + 2H^+ \quad (4)$$

XRD patterns in this study were unable to detect Pb metaphosphate, i.e., $(Pb(PO_3)_2)_n$, possibly because they existed in amorphous form. Ohashi and Yamagishil (1960) [54] found that $(KPO_3)_n$ could react with various metal ions (Na^+, Ca^{2+}, Mg^{2+}, Cu^{2+}, Pb^{2+} and Ni^{2+}) through ion exchange reaction, and the Ni-substituted product dried at 110°C was completely amorphous.

SEM images showed pea-pod-shaped aggregates on the surface of Pb-loaded BCP, and EDS analysis confirmed abundant C, O, Pb and P in these aggregates, but no measurable contents of K and other elements (Fig. 7). The atomic ratio of P/Pb in BCP was higher than 5:3 (Fig. 7), suggesting the likely formation of $[Pb(PO_3)_2]_n$ during Pb(II) adsorption on BCP. A high atomic ratio of P/Pb was observed in BCP500+Pb and BCP700+Pb, which were probably derived from the nonreactive C-P or C-O-P groups.

Results indicated that $(KPO_3)_n$ played important roles in enhanced adsorption of Pb(II) on BCP. BCP300 had the lowest P content (4.14%, Table 1), but showed the highest Pb(II)

adsorption capacity. There are three possible reasons for this result. Firstly, the size of $(KPO_3)_n$ particles increased with rising pyrolysis temperature (Fig. 1), indicating a shorter chain length of $(KPO_3)_n$ in BCP300. In BCP300, $(KPO_3)_n$ and its derivate ($K_aM_{(n-a)/x}(PO_3)_n$) could have bigger dissociation degree than other BCP, and hence higher exchange constant of $(KPO_3)_n$ with Pb(II) and other metals [55]. Secondly, low pH condition in BCP300 might have favored the hydrolysis of polymetaphosphate into orthophosphate [56], and the rate of hydrolysis decreased with increasing polymetaphosphate chain length [57], thus forming lead orthophosphate (e.g., $Pb_5(PO_4)_3OH$). Finally, C-P compounds were formed through P-O-C and C-P bonds in BCP500 and BCP700, but they had a weaker ability to form precipitate with Pb(II) than soluble $(PO_3^-)_n$ species [30].

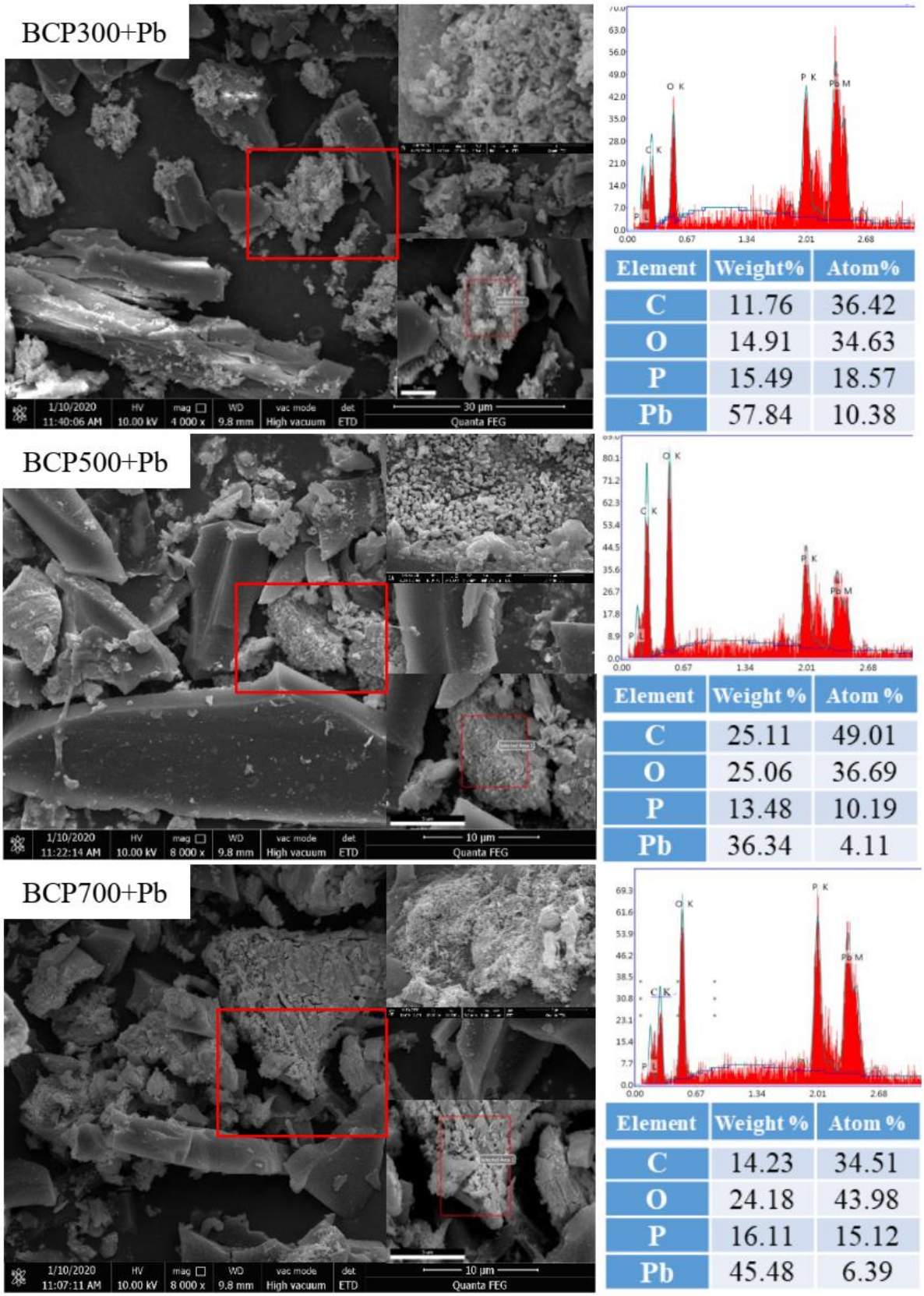

Fig. 7 SEM micrographs and EDS analysis of Pb-loaded BCP

392 3.4 Environmental implications

393 BCP proved to be a promising adsorbent to remove Pb(II) from water bodies at high initial
394 Pb(II) concentration (≥200 mg L^{-1}). The crystalline $(KPO_3)_n$ is practically insoluble in water,
395 but it may become soluble in dilute alkali metal solutions (e.g., Na^+, Ca^{2+}, and Mg^{2+}) owing to
396 the formation of mixed polymetaphosphate, i.e., $K_aM_{(n-a)/x}(PO_3)_n$, where M= Na, Mg or Ca, and
397 x is valence state of these metal ions (1 or 2) [58]. Low concentration of alkali metal ions (Na^+,
398 Ca^{2+}, and Mg^{2+}) were detected in water extract of BCP (Table S4), and about 50 mg L^{-1} P was
399 also detected (Fig. S4). When the added Pb(II) concentration was low (≤100 mg L^{-1}), the P
400 concentration remained almost unchanged, while it proportionately decreased with the quantity
401 of adsorbed Pb(II) until approaching zero (Fig. S4). By contrast, K concentration in solution
402 was almost unchanged at low Pb(II) concentration (≤100 mg L^{-1}), and then it increased at high
403 Pb(II) concentration (Fig. S4). Therefore, the quantity of dissolved $K_aM_{(n-a)/x}(PO_3)_n$ in aqueous
404 solution from BCP was much higher than that of Pb(II). Only a small portion of metal ions in
405 $K_aM_{(n-a)/x}(PO_3)_n$ would be replaced by Pb(II) to form $K_bPb_cM_{(n-2b-c)/x}(PO_3)_n$ (b<a) that is still
406 soluble; when more alkali metals are further replaced at high levels of Pb(II), this compound
407 would precipitate. Similar results were found by McElroy et al. (1965) [59] who studied the
408 reactions between Fe^{3+} and $(NaPO_3)_n$. Moreover, the increasing Pb(II) adsorption at low
409 concentration of Fe^{3+} and Cu^{2+} (Fig. 6) confirmed that replacement of alkali metals promoted
410 the formation of precipitates. The precipitation of Pb(II) depended on the mole ratio of
411 Pb(II)/metal ions in the aqueous solution. Therefore, the application of BCP in treating
412 wastewater containing abundant cations, such as K^+, Ca^{2+}, Mg^{2+}, Mn^{2+}, and $Fe^{2+/3+}$, needs to be
413 investigated in the future.

414 $(KPO_3)_n$ could also complex with various multivalent metal ions (Mn^{2+}, Co^{2+}, Ni^{2+}, Cu^{2+},
415 Fe^{3+}, Pb^{2+}) to form precipitates, whereas the reaction rates and conversions would be distinct
416 between them [52]. Hence, more research should be done to explore the application of BCP in

adsorbing other heavy metals. Biochar is an effective soil amendment for reducing nutrient leaching [60] and $(KPO_3)_n$ is a good slow-release fertilizer [61], thus, the potential application of BCP as fertilizer in soil is also worth further studying.

4. Conclusions

In this study, novel phosphorus-modified biochars were prepared by the co-pyrolysis of poplar sawdust with KH_2PO_4, and used for Pd(II) removal from water. The modification with KH_2PO_4 greatly reduced the carbon loss (residual carbon increased by 4.04%, 16.56%, and 23.50% for BCP300, BCP500, and BCP700, respectively) in the biochar and negatively affect porous structure (BET surface area decreased by 41.53%, 80.32%, and 59.74% for BCP300, BCP500, and BCP700, respectively), possibly resulting from the formation of C-O-P and/or C-P groups. Crystalline $(KPO_3)_n$ were uniformly dispersed on the surface of KH_2PO_4-modified biochars. Compared with original biochar, BCP samples showed an increased Pb(II) adsorption capacity (q_{max} increased by 5.37, 2.36, and 0.61 times for BCP300, BCP500, and BCP700, respectively) at high Pb(II) concentration (> 100 mg L^{-1}), which resulted from the formation of precipitates including $[Pb(PO_3)_2]_n$, $Pb_5(PO_4)_3OH$ and $PbHPO_4$. Regardless of the pyrolysis temperature, BCP showed almost no adsorption capacity of Pb(II) at low Pb(II) concentration (≤100 mg L^{-1}). Therefore, special attention should be paid when using the KH_2PO_4-modified biochar to treat water with low Pb(II) concentration. BCP300 was found the most suitable adsorbent for Pb(II) removal (q_{max} =154.7 mg g^{-1}), which mainly resulted from short chain length of $(KPO_3)_n$. Overall, the KH_2PO_4-modified biochar can serve as an efficient remediation agent for wastewater with severe Pb(II) pollution.

Acknowledgements

This work was supported by Huai'an Research Program of Basic Research and Frontier Technology (NO. HABZ201802).

References

[1] S. Yao, J. Zhang, D. Shen, R. Xiao, S. Gu, M. Zhao, J. Liang, Removal of Pb(II) from water by the activated carbon modified by nitric acid under microwave heating, J. Colloid. Interface. Sci. 463 (2016) 118–127.

[2] G.H. Kumar, J.P. Kumari, Heavy metal lead influative toxicity and its assessment in phytoremediating plants—a review, Water. Air. Soil. Poll. 226 (2015) 1-11.

[3] K.H. Vardhan, P.S. Kumar, R.C. Panda, A review on heavy metal pollution, toxicity and remedial measures: Current trends and future perspectives, J. Mol. Liqu. 290 (2019) 111197.

[4] H. Xu, L. Li, H. Lv, X. Liu, H. Jiang, pH-dependent phosphatization of ZnO nanoparticles and its influence on subsequent lead sorption, Environ. Poll, 208 (2016) 723-731.

[5] A.B. Nastasovic, B.M. Ekmescic, Z. P. Sandic, D. V. Randelovic, M. Mozetic, A. Vesel, A.E. Onjiad, Mechanism of Cu(II), Cd(II) and Pb(II) ions sorption from aqueous solutions by macroporous poly(glycidyl methacrylate-co-ethylene glycol dimethacrylate), Appl. Surf. Sci. 385 (2016) 605-615.

[6] S.A. Sajjadi, A. Meknati, E.C. Lima, G.L. Dotto, D.I. Mendoza-Castillo, I. Anastopoulos, F. Alakhras, E.I. Unuabonah, P. Singh, A. Hosseini-Bandegharaei, A novel route for preparation of chemically activated carbon from pistachio wood for highly efficient Pb(II) sorption, J. Environ. Manage. 236 (2019) 34-44.

[7] M.I. Inyang, B. Gao, Y. Yao, Y. Xue, A. Zimmerman, A. Mosa, P. Pullammanappallil, Y.S. Ok, X. Cao, A review of biochar as a low-cost adsorbent for aqueous heavy metal removal, Crit. Rev. Env. Sci. Tec. 46 (2016) 406-433.

[8] M.B. Ahmed, J.L. Zhou, H.H. Ngo, W. Guo, M. Chen, Progress in the preparation and application of modified biochar for improved contaminant removal from water and wastewater. Bioresour. Technol. 214 (2016) 836–851.

[9] R. Li, H. Deng, X. Zhang, J.J. Wang, M.K. Awasthi, Q. Wang, R. Xiao, B. Zhou, J. Du, Z. Zhang, High-efficiency removal of Pb(II) and humate by a CeO2-MoS2 hybrid magnetic

biochar. Bioresour. Technol. 273 (2019) 335–340.

[10] D. Mohan, A. Sarswat, Y.S. Ok, P.C. Jr, Organic and inorganic contaminants removal from water with biochar, a renewable, low cost and sustainable adsorbent–a critical review. Bioresour. Technol. 160 (2014) 191-202.

[11] H.K.S. Panahi, M. Dehhaghi, Y.S. Ok, A.S. Nizami, B. Khoshnevisan, S.I. Mussatto, M. Aghbashlo, M. Tabatabari, S.S. Lam, A comprehensive review of engineered biochar: production, characteristics, and environmental applications. J. Clean. Prod. 270 (2020) 122462.

[12] Q. Abbas, G. Liu, B. Yousaf, M. U. Ali, H. Ullah, M. A. M. Munir, R. Liu, Contrasting effects of operating conditions and biomass particle size on bulk characteristics and surface chemistry of rice husk derived-biochars, J. Anal. Appl. Pyrol. 134 (2018) 281-292.

[13] J.A. Rodriguez, J.F.L. Filho, L.C.A. Melo, I.R.D. Assis, T. S. de Oliveira, Influence of pyrolysis temperature and feedstock on the properties of biochars produced from agricultural and industrial wastes, J. Anal. Appl. Pyrol. 149 (2020) 104839.

[14] S. Mandal, B. Sarkar, N. Bolan, J. Novak, Y. S. Ok, L. V. Zwieten, B P. Singh, M B. Kirkham, G. Choppala, K. Spokas, R. Naidu, Designing advanced biochar products for maximizing greenhouse gas mitigation potential, Crit. Rev. Environ. Sci. Technol. 46 (2016) 1367-1401.

[15] J. Wang, S. Wang, Preparation, modification and environmental application of biochar: A review. J. Clean. Prod. 227 (2019) 1002-1022.

[16] Y. Huang, S. Li, J. Chen, X. Zhang, Y. Chen, Adsorption of Pb(II) on mesoporous activated carbons fabricated from water hyacinth using H_3PO_4 activation: adsorption capacity, kinetic and isotherm studies, Appl. Surf. Sci. 293 (2014) 160-168.

[17] H. Peng, P. Gao, G. Chu, B. Pan, J. Peng, B. Xing, Enhanced adsorption of Cu(II) and Cd(II) by phosphoric acid-modified biochars, Environ. Poll. 229 (2017) 846-853.

[18] Q. Jiang, W. Xie, S. Han, Y. Wang, Y. Zhang, Enhanced adsorption of Pb(II) onto modified hydrochar by polyethyleneimine or H_3PO_4: An analysis of surface property and interface mechanism, Colloid. Surface. A. 583 (2019) 123962.

[19] S. Zhang, H. Zhang, J. Cai, X. Zhang, J. Zhang, J. Shao, Evaluation and prediction of cadmium removal from aqueous solution by phosphate-modified activated bamboo biochar, Energ. Fuel. 32 (2018) 4469–4477.

[20] R. Gao, Q. Fu, H. Hu, Q. Wang, Y. Liu, J. Zhu, Highly-effective removal of Pb by co-pyrolysis biochar derived from rape straw and orthophosphate, J. Hazard. Mater. 371 (2019) 191–197.

[21] B.U. Grzmil, B. Kic, Potassium, sodium, and calcium polyphosphates with controlled solubility, J. Agr. Food. Chem. 43(1995), 2463-2470.

[22] K.S. Lee, Hidden nature of the high-temperature phase transitions in crystals of KH_2PO_4-type: is it a physical change? J. Phys. Chem. Solids. 57(1996) 333-342.

[23] J.R. Van Wazer, C.F. Callis, Metal complexing by phosphates. J. Am. Chem. Soc. 80 (1958) 1011–1046.

[24] R. Jastrzab, L. Lomozik, Stability and coordination mode of complexes of polyphosphates and polymetaphosphates with copper(II) ions in aqueous solution—potentiometric, spectral and theoretical studies, J. Solution. Chem. 39(2010) 909-919.

[25] M.P. Gatabi, H.M. Moghaddam, M. Ghorbani, Point of zero charge of maghemite decorated multiwalled carbon nanotubes fabricated by chemical precipitation method. J. Mol. Liq. 216 (2016) 117-125.

[26] GB/T 12496.3-1999. Test method of wooden activated carbon-Determination of ash content.

[27] H. Ettoumi, T. Mhiri, Kinetic process of dehydration at fusion temperature and the high-temperature phase transition in KH_2PO_4, J. Mol. Struct. 1034 (2013), 112–118.

[28] L. Zhao, X. Cao, W. Zheng, Y. Kan, Phosphorus-assisted biomass thermal conversion: reducing carbon loss and improving biochar stability. Plos One, 9(2014), e115373.

[29] F. Li, X. Cao, L. Zhao, J. Wang, Z.L. Ding, Effects of mineral additives on biochar formation: Carbon retention, stability, and properties, Environ. Sci. Technol. 48 (2014) 11211−11217.

[30] L. Zhao, X. Cao, W. Zheng, J.W. Scott, B.K. Sharma, X. Chen, Co-pyrolysis of biomass with phosphate fertilizers to improve biochar carbon retention, slow nutrient release, and stabilize heavy metals in soil, ACS. Sustain. Chem. Eng. 4 (2016) 1630-1636.

[31] X.B. Xu, X. Hu, Z.H. Ding, Y.J. Chen, Effects of copyrolysis of sludge with calcium carbonate and calcium hydrogen phosphate on chemical stability of carbon and release of toxic elements in the resultant biochars, Chemosphere. 189 (2017) 76−85.

[32] P. Boguta, Z. Sokołowska, K. Skic, A.Tomczyk, Chemically engineered biochar–effect of concentration and type of modifier on sorption and structural properties of biochar from wood waste. Fuel. 256(2019), 115893.

[33] H. Li, X. Dong, E.B. da Silva, L.M. de Oliveira, Y. Chen, L.Q. Ma, Mechanisms of metal sorption by biochars: biochar characteristics and modifications, Chemosphere. 178 (2017) 466-478.

[34] J.H. Kwak, M.S. Islam, S. Wang, S.A. Messele, M.A. Naeth, M.G. El-Din, S.X. Chang, Biochar properties and lead(II) adsorption capacity depend on feedstock type, pyrolysis temperature, and steam activation, Chemosphere. 231 (2019) 393-404.

[35] R. R. Domingues, P. F. Trugilho, C. A. Silva, M. I. C. N. A. De, L. C. A. Melo, Z. M. Magriotis, M. A. Sánchez-Monedero, Properties of biochar derived from wood and high-nutrient biomasses with the aim of agronomic and environmental benefits. PLoS ONE, 12(2017), e0176884.

[36] E. Smidt, M. Schwanninger, Characterization of waste materials using ftir spectroscopy:

process monitoring and quality assessment, Spectrosc. Lett. 38 (2005) 247-270.

[37] A. Jouini, M. Férid, M. Trabelsi-Ayadi, Equilibrium diagram of KPO_3-$Y(PO_3)_3$system, chemical preparation and characterization of $KY(PO_3)_4$, Thermochim. Acta. 400 (2003) 199-204.

[38] A. Shaim, M.M. Et-tabirou, Role of titanium in sodium titanophosphate glasses and a model of structural units, Chem. Phys. 80 (2003) 63-67.

[39] P.K. Jha, O.P. Pandey, K. Singh, FTIR spectral analysis and mechanical properties of sodium phosphate glass–ceramics, J. Mol. Struct. 1083 (2015) 278-285.

[40] P. Shenoy, K.V. Bangera, G.K. Shivakumar, Growth and thermal studies on pure ADP, KDP and mixed $K_{1-x}(NH_4)_xH_2PO_4$ crystals, Cryst. Res. Technol. 45 (2010) 825-829.

[41] J. Niu, Z. Zhang, D. Jiang, Investigation of phase evolution during the formation of calcium potassium sodium orthophosphate, Mater. Chem. Phys. 78 (2003) 308-312.

[42] A. Downie, A. Crosky, P. Munroe Physical properties of biochar J. Lehmann, S. Joseph (Eds.), Biochar for Environmental Management, Earthscan, London (2009), 13-32.

[43] Y. Wang, Y. Hu, X. Zhao, S. Wang, G. Xing, Comparisons of biochar properties from wood material and crop residues at different temperatures and residence times, Energ. Fuel. 27 (2013) 5890–5899.

[44] Y. Chen, B. Wang, J. Xin, P. Sun, D. Wu, Adsorption behavior and mechanism of Cr(VI) by modified biochar derived from *Enteromorpha prolifera*, Ecotox. Environ. Safe. 164 (2018) 440-447.

[45] T. Depci, A.R. Kul, Y. Önal, Competitive adsorption of lead and zinc from aqueous solution on activated carbon prepared from van apple pulp: study in single- and multi-solute systems, Chem. Eng. J. 200-202 (2012) 224-236.

[46] Y. Qiu, H. Cheng, C. Xu, D. Sheng, Surface characteristics of crop-residue derived black carbon and lead(II) adsorption, Water Res. 42 (2008) 567–574.

[47] M. Jalali, F. Aboulghazi, Sunflower stalk, an agricultural waste, as an adsorbent for the removal of lead and cadmium from aqueous solutions, J. Mater. Cycles. Waste. 15 (2013) 548–555.

[48] L. Liu, Y. Huang, S. Zhang, Y. Gong, Y. Su, J. Cao, H. Hu, Adsorption characteristics and mechanism of Pb(II) by agricultural waste-derived biochars produced from a pilot-scale pyrolysis system, Waste. Manage. 100(2019) 287-295.

[49] J.H. Kwak, M. S. Islam, S. Wang, S.A. Messele, M. A. Naeth, M. G. El-Din, S. X. Chang. Biochar properties and lead(II) adsorption capacity depend on feedstock type, pyrolysis temperature, and steam activation, Chemosphere 231(2019) 393-404.

[50] J. Ifthikar, J. Wang, Q. Wang, T. Wang, H. Wang, A. Khan, A. Jawad, T. Sun, X. Jiao, Z. Chen, Highly efficient lead distribution by magnetic sewage sludge biochar: sorption mechanisms and bench applications, Bioresour. Technol. 238 (2017) 399–406.

[51] X. Xu, X. Cao, L. Zhao, H. Zhou, Q. Luo, Interaction of organic and inorganic fractions of biochar with Pb(II) ion: further elucidation of mechanisms for Pb(II) removal by biochar. RSC Adv. 4(2014) 44930e44937.

[52] R. Wang, D. Huang, Y. Liu, C. Zhang, C. Lai, G. Zeng, M. Cheng, X. Gong, J. Wan, H. Luo, Investigating the adsorption behavior and the relative distribution of Cd^{2+} sorption mechanisms on biochars by different feedstock, Bioresour Technol. 261 (2018) 265–271.

[53] E.S. Penido, L.C.A. Melo, L.R.G. Guilherme, M.L. Bianchi, Cadmium binding mechanisms and adsorption capacity by novel phosphorus/magnesium-engineered biochars, Sci. Total. Environ. 671 (2019) 1134-1143.

[54] S. Ohashi, K. Yamagishi, Long-chain Phosphates. I. Reactions of solid potassium kurrol salt with solutions of various metal salts, B. Chem. Soc. Jap. 33 (1960) 1431–1435.

[55] E. Thilo, Condensed phosphates and arsenates, Adv. Inorg. Chem. Rad. 4 (1962) 1-75.

[56] L.J. Anghileri, Hydrolysis of sodium polymetaphosphate and sodium pyrophosphate under the influence of temperature and pH, Int. J. Appl. Radiat. Isot. 15 (1964) 549-551.

[57] R.P. Dick, M.A. Tabatabai, Hydrolysis of polyphosphates in soils, Soil. Sci. 142 (1986) 132-140.

[58] C.C. Volkerding, R. Bradfield, The solubility and reversion of calcium and potassium metaphosphates, Soil. Sci. Soc. Am. J. 8 (1944) 159-166.

[59] S.M.K. McElroy, J.F. Hazel, W.M. McNabb, Reactions between iron (III) ions and glassy polyphosphates, J. Inorg. Nucl. Chem. 27 (1965) 859-866.

[60] H. Yuan, T. Lu, Y. Wang, Y. Chen, T. Lei, Sewage sludge biochar: Nutrient composition and its effect on the leaching of soil nutrients, Geoderma. 267 (2016) 17-23.

[61] J. Hagin, Evaluation of potassium metaphosphate as fertilizer, Soil. Sci. 102 (1966) 373-379.

Supplementary Information for:

Influence of pyrolysis temperature on the characteristics and lead(II) adsorption capacity of phosphorus-engineered poplar sawdust biochar

Yonggang Xu[a], Tianxia Bai[b], Qiao Li[c], Hongtao Yang[d],Yubo Yan[b*], Binoy Sarkar[e*], Su Shiung Lam[f], Nanthi Bolan[g]

[a]*Jiangsu Key Laboratory for Eco-Agricultural Biotechnology around Hongze Lake/ Collaborative Innovation Center of Regional Modern Agriculture & Environmental Protection, Huaiyin Normal University, Huai'an, 223300, China*

[b]*School of Chemistry and Chemical Engineering, Huaiyin Normal University, Huai'an, 223300, China*

[c]*School of Environmental and Biological Engineering, Nanjing University of Science and Technology, Nanjing 210094, China*

[d]*Xi'an Modern Chemistry Research Institute, Xi'an 71065, PR China*

[e]*Lancaster Environment Centre, Lancaster University, Lancaster, LA1 4YQ, United Kingdom*

[f]*Pyrolysis Technology Research Group, Institute of Tropical Aquaculture and Fisheries (AKUATROP) & Institute of Tropical Biodiversity and Sustainable Development (Bio-D Tropika), Universiti Malaysia Terengganu, 21030 Kuala Nerus, Terengganu, Malaysia*

[g]*Faculty of Science, The University of Newcastle, University Drive, Callaghan, NSW 2308, Australia*

***Corresponding author:**

Dr Yubo Yan (yubo.yan@hytc.edu.cn); Dr Binoy Sarkar (b.sarkar@lancaster.ac.uk)

The pseudo-first-order (Eq. 1) and pseudo-second-order (Eq. 2) models were used to describe the adsorption kinetic data. The initial adsorption rate v_0 of the pseudo-second-order model is represented by Eq. 3.

$$Q_t = Q_e(1-e^{-k_1 t}) \quad (1)$$

$$Qt = (Q_e^2 k_2 t)/(1+Q_e k_2 t) \quad (2)$$

$$v_0 = k_2 Q_e^2 \quad (3)$$

where Q_t (mg g^{-1}) and Q_e (mg g^{-1}) are the amounts of Pb(II) adsorbed at time t and at equilibrium, respectively, k_1 (h^{-1}) represents the rate constant of pseudo-first-order model, and k_2 is the rate constant of the pseudo second-order model (g mg^{-1} h^{-1}).

The Langmuir (Eq. 4) and Freundlich (Eq. 5) model were appled to simulate the adsorption isotherm data.

$$Q_e = K_L q_{max} C_e/(1+ K_L C_e) \quad (4)$$

where Q_e (mg g^{-1}) and C_e (mg L^{-1}) are the adsorbed amount of Pb(II) by biochar and Pb(II) concentration at equilibrium solution, K_L (L mg^{-1}) is the Langmuir affinity constant, and q_{max} (mg g^{-1}) is the theoretical maximum adsorption capacity as the monolayer surface is completely covered.

$$Q_e = K_F C_e^n \quad (5)$$

where K_F [(mg g^{-1}) (L mg^{-1})$^{1/n}$] and n are the constants related to adsorption capacity and intensity, respectively.

The data were adjusted to kinetic mathematical equations and sorption isotherm equations, which were evaluated through the coefficient of determination (R^2) and Chi-square (χ^2) values. The χ^2 test measures the difference between the experimental and equations data, and is mathematically expressed by Eq. 6.

$$\chi 2 = \sum_{i=1}^{N} \frac{(q_e, \exp - q_e, \mathrm{cal})^2}{q_e, \mathrm{cal}} \quad (\mathrm{Eq.}\ 6)$$

where q_e, exp corresponds to the amount of solute adsorbed in the experimental data at equilibrium, and q_e, cal is the quantity adsorbed at equilibrium through the model. A smaller value of χ^2 indicates a better fit of the experimental data to the equations.

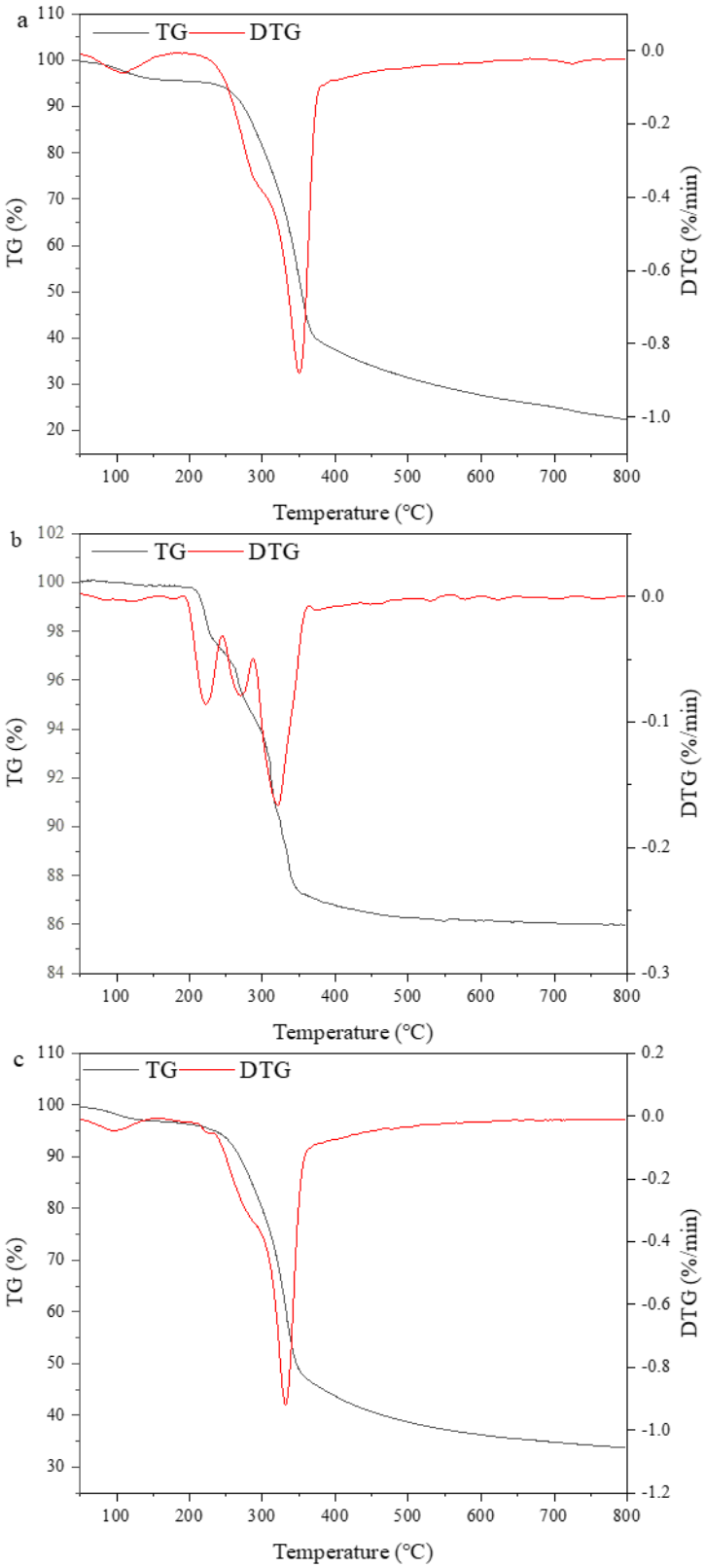

Fig. S1 TG and DTG of poplar sawdust (a), KH_2PO_4 (b), and mixture (c)

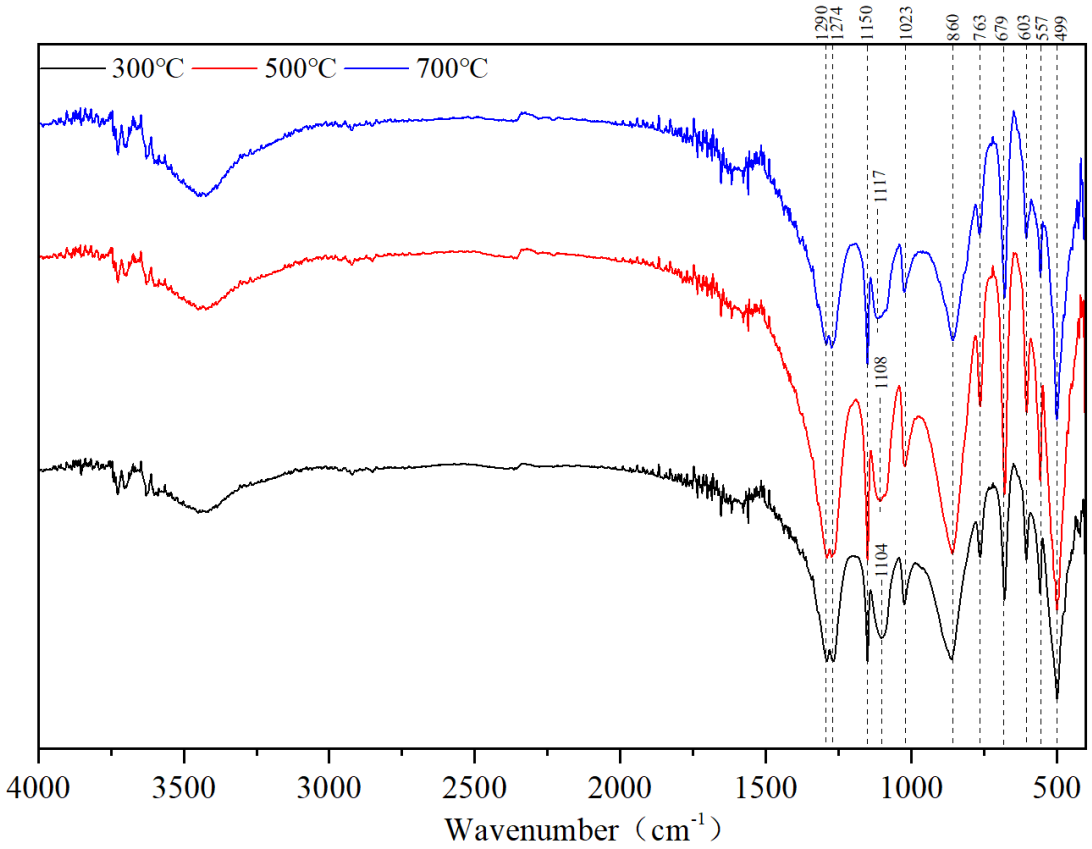

Fig. S2 FTIR of the thermal production of KH_2PO_4 at 300 ℃, 500 ℃ and 700 ℃

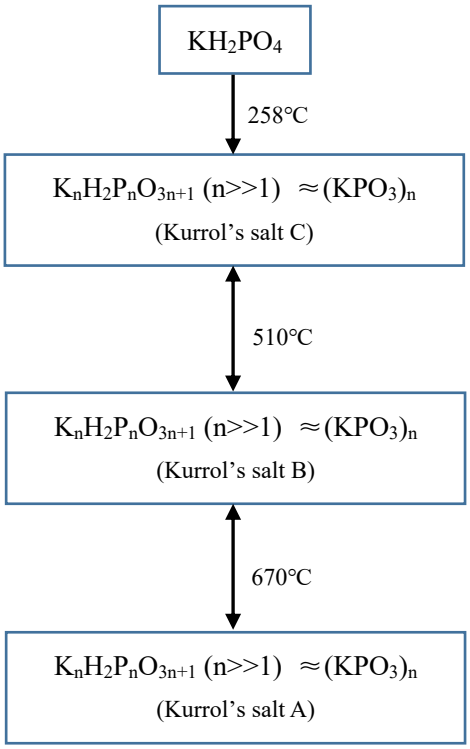

Fig. S3 The condensed phosphates prepared by heating KH_2PO_4 and their interrelationships (Lee, 1996)

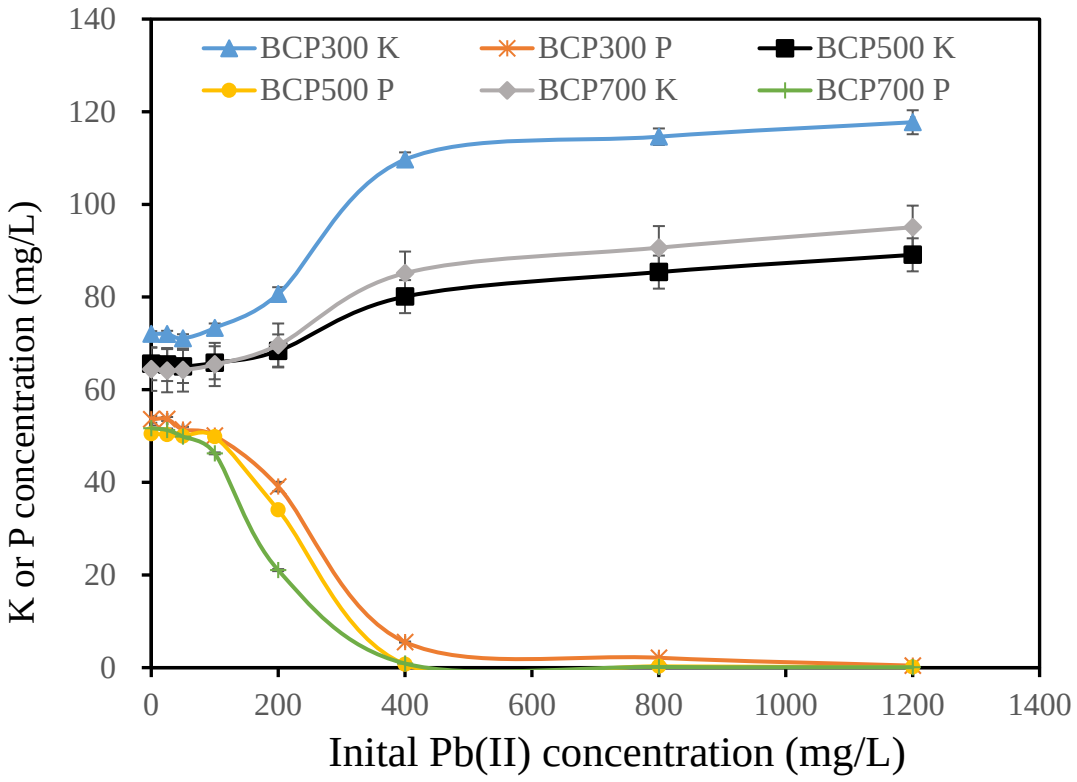

Fig. S4 The change of K and P concentrations in aqueous solution with the added Pb(II) concentration

Table S1 The characteristics of poplar sawdust

Sample	Lignocellulosic composition (%)			Ultimate analyses (%)				Proximate analyses (%)			
	cellulose	hemicellulose	lignin	C	H	N	O	Volatile matter	Fixed carbon	Ash	Water content
Poplar sawdust	40.05	19.38	28.78	51.40	3.69	0.74	30.2	70.68	21.62	3.31	4.39

Table S2 The porous characteristics of biochars

	BET surface area (m^2 g^{-1})	Micropore surface area[a] (m^2 g^{-1})	Total pore volume[b] (cm^3 g^{-1})	Microporous pore volume[c] (cm^3 g^{-1})	Average pore diameter (nm)
BC300	3.01	-	0.006	-	8.24
BCP300	1.76	-	0.005	-	11.1
BC500	31.0	10.4	0.028	-	3.62
BCP500	6.10	-	0.012	0.005	7.89
BC700	303	212	0.182	0.149	2.40
BCP700	122	89.0	0.079	0.066	3.57

a Microporous surface area, calculated from the t-plot method.

b Total pore volume, obtained from single point adsorption at relative pressure close to 0.995.

c Microporous pore volume, calculated from the t-plot method.

Table S3 Comparison of maximum adsorption capacity of Pb(II) on modified-biochar

Feedstocks	Modification	Pyrolysis temperature (°C)	pH	dosage (g/L)	Initial concentration (mg L^{-1})	Adsorption capacity (mg g^{-1})	References
Oak bark	Magnetization	400	5.0	3.0	1-100	30.20	Mohan et a., 2014
Oak wood	Magnetization	400	5.0	3.0	1-100	10.13	
Camphor leaf	Ultrasonic with NaOH	450	5.8	4.0	50-1000	98.33	Wang et al., 2018
Camellia seed husk	Soaking by HCl	700	5.0	1.0	0-300	109.67	Wu et al., 2019
Lemna minor	H_3PO_4 activation	500	6.0	0.2	1-40	170.9	Huang et al., 2014
Canola straw	Steam activation	700	Not adjustion	1.0	50-200	195.00	Kwak et al., 2019
Pistachio wood	NaOH	800	6.0	0.1	7.5-22.5	190.2	Sajjadi et al., 2019
Poplar sawdust	KH_2PO_4 modification	300	5.0	5.0	25-1200	143.28	This study

Table S4 The concentration of water-extractable Na^+, Ca^{2+} and Mg^{2+} from BCP (5 g L^{-1})

	Na^+ (mg L^{-1})	Ca^{2+} (mg L^{-1})	Mg^{2+} (mg L^{-1})
BCP300	3.20	13.97	2.60
BCP500	3.95	16.83	3.02
BCP700	2.23	17.73	2.91

Reference

Chongqing, W., Hui, W., Yijun, C., 2018. Pb(II) sorption by biochar derived from *Cinnamomum camphora* and its improvement with ultrasound-assisted alkali activation. Colloid. Surface. A. 556, 177-184.

Huang, Y., Li, S., Lin, H., Chen, J., 2014. Fabrication and characterization of mesoporous activated carbon from *Lemna minor* using one-step H_3PO_4 activation for Pb(II) removal. Appl. Surf. Sci. 317, 422-431.

Kwak, J.H., Islam, M.S., d, Wang, S., Messele, S.A., Naeth, M.A., El-Din, M.G., Chang, S.X., 2019. Biochar properties and lead(II) adsorption capacity depend on feedstock type, pyrolysis temperature, and steam activation. Chemosphere. 231, 393-404.

Lee, K.S., 1996. Hidden nature of the high-temperature phase transitions in crystals of KH2PO4-type: is it a physical change? J. Phys. Chem. Solids. 57(3), 333-342.

Mohan, D., Kumar, H., Sarswat, A., Alexandre-Franco, M., & Pittman, C. U., 2014. Cadmium and lead remediation using magnetic oak wood and oak bark fast pyrolysis bio-chars. Chem. Eng. J. 236(2), 513-528.

Sajjadi, S.A., Meknati A., Lima E.C., Dotto, G.L., Mendoza-Castillo, D.I., Anastopoulos, I., Alakhras, F., Unuabonah, E.I., Singh, P., Hosseini-Bandegharaei, A., 2019. A novel route for preparation of chemically activated carbon from pistachio wood for highly efficient Pb(II) sorption. J. Environ. Manage. 236, 34-44.

Wu, J., Wang, T., Zhang, Y., W.P., 2019. The distribution of Pb(II)/Cd(II) adsorption mechanisms on biochars from aqueous solution: Considering the increased oxygen functional groups by HCl treatment. Bioresour. Technol. 291, 121859.